Correcting Propagation Effects in C-Band Polarimetric Radar Observations of Tropical Convection Using Differential Propagation Phase

LAWRENCE D. CAREY, STEVEN A. RUTLEDGE, AND DAVID A. AHIJEVYCH

Department of Atmospheric Science, Colorado State University, Fort Collins, Colorado

TOM D. KEENAN

Bureau of Meteorology Research Centre, Melbourne, Australia

(Manuscript received 21 April 1999, in final form 11 October 1999)

ABSTRACT

A propagation correction algorithm utilizing the differential propagation phase (ϕ_{dp}) was developed and tested on C-band polarimetric radar observations of tropical convection obtained during the Maritime Continent Thunderstorm Experiment. An empirical procedure was refined to estimate the mean coefficient of proportionality a (b) in the linear relationship between ϕ_{dp} and the horizontal (differential) attenuation throughout each radar volume. The empirical estimates of these coefficients were a factor of 1.5–2 times larger than predicted by prior scattering simulations. This discrepancy was attributed to the routine presence of large drops [e.g., differential reflectivity $Z_{dr} \geq 3$ dB] within the tropical convection that were not included in prior theoretical studies.

Scattering simulations demonstrated that the coefficients a and b are nearly constant for small to moderate sized drops (e.g., $0.5 \leq Z_{dr} \leq 2$ dB; 1 ≤ diameter $D_0 < 2.5$ mm) but actually increase with the differential reflectivity for drop size distributions characterized by $Z_{dr} > 2$ dB. As a result, large drops 1) bias the mean coefficients upward and 2) increase the standard error associated with the mean empirical coefficients down range of convective cores that contain large drops. To reduce this error, the authors implemented a ''large drop correction'' that utilizes enhanced coefficients a^* and b^* in large drop cores.

Validation of the propagation correction algorithm was accomplished with cumulative rain gauge data and internal consistency among the polarimetric variables. The bias and standard error of the cumulative radar rainfall estimator $R(Z_h)$ $[R(K_{dp}, Z_{dr})]$, where Z_h is horizontal reflectivity and K_{dp} is specific differential phase, were substantially reduced after the application of the attenuation (differential attenuation) correction procedure utilizing ϕ_{dp}. Similarly, scatterplots of uncorrected Z_h (Z_{dr}) versus K_{dp} substantially underestimated theoretical expectations. After application of the propagation correction algorithm, the bias present in observations of both $Z_h(K_{dp})$ and $Z_{dr}(K_{dp})$ was removed and the standard errors relative to scattering simulation results were significantly reduced.

1. Introduction

a. Background material

The need to correct higher-frequency (e.g., C band) radar reflectivity for attenuation effects has long been recognized (Ryde 1946; Atlas and Banks 1951; Hitschfeld and Bordan 1954; Gunn and East 1954). There are many examples in the scientific literature of severe attenuation effects at C band that render the radar reflectivity data nearly useless for quantitative and even qualitative interpretation (e.g., Johnson and Brandes 1987; Shepherd et al. 1995).

A reliable empirical estimate of attenuation has proven elusive. Hitschfeld and Bordan (1954) demonstrated that an indirect estimate of the specific attenuation A can be obtained from empirical Z–R (reflectivity vs rain rate) and A–R (attenuation vs rain rate) relationships. In their technique, the correction for attenuation at the nth gate is accomplished using the reflectivity measurements made at all preceding $n - 1$ gates, beginning with the gate closest to the radar. Hitschfeld and Bordan (1954) concluded that even a small error in the radar power calibration could cause a large error in the corrected reflectivity. Indeed, this error, which accumulates as the correction is successively carried out in range, can be larger than the original error caused by attenuation, rendering reflectivity-based attenuation correction futile (e.g., Hitschfeld and Bordan 1954; Hildebrand 1978; Johnson and Brandes 1987).

With the development of polarization diverse radars (e.g., Bringi and Hendry 1990), a better estimate of attenuation is possible than with reflectivity alone. Ay-

Corresponding author address: Dr. Lawrence D. Carey, Department of Atmospheric Science, Colorado State University, Fort Collins, CO 80521.
E-mail: carey@olympic.atmos.colostate.edu

din et al. (1989) derived an empirical relationship to estimate the specific horizontal attenuation (A_h, dB km^{-1}) based on the horizontal reflectivity (Z_h, dBZ) and the differential reflectivity (Z_{dr}, dB), which is less sensitive to variations in the drop size distribution (DSD) than past relationships relying on Z_h alone. Gorgucci et al. (1996, 1998) recently modified and extended this method to include a correction for the differential attenuation ($\alpha_{hv} = \alpha_h - \alpha_v$, dB) at C band, where α_h and α_v are the attenuation at horizontal and vertical polarizations, respectively, through a rain medium. Except for the empirical relationship relating α_h (or α_{hv}) to the radar measurements, attenuation (or differential attenuation) correction schemes utilizing Z_h and Z_{dr} are similar to the original procedure of Hitschfeld and Bordan (1954) and therefore suffer from some of the same sensitivities and biases, including power calibration errors (Aydin et al. 1989; Gorgucci 1996, 1998).

Holt (1988) and Bringi et al. (1990) proposed an alternative approach to correct Z_h (Z_{dr}) for the deleterious effects of α_h (α_{hv}) that utilizes an estimate of the differential propagation phase (ϕ_{dp}) through rain. The differential propagation phase represents the difference in the phase shift between horizontally and vertically polarized waves as they propagate through a rain medium (e.g., Oguchi 1983). Holt (1988) and Bringi et al. (1990) demonstrated that α_{hv} and α_h are approximately linearly proportional to ϕ_{dp} at precipitation radar frequencies (3–10 GHz). This approach has two distinct advantages over the power-based methods discussed above. The differential propagation phase is 1) unaffected by attenuation as long as the returned power is above the noise power and 2) independent of radar calibration errors (e.g., Zrnić and Ryzhkov 1996).

The accuracy of the correction procedure is affected by 1) variability in the drop size distribution (Bringi et al. 1990; Jameson 1991a; Zrnić et al. 2000; Keenan et al. 2000, hereinafter KCZM), 2) deviations from the assumed temperature (Jameson 1992; Aydin and Giridhar 1992), 3) departures from the postulated drop shape versus size relationship (KCZM) 4) nonzero values of the backscatter differential phase (δ) between horizontal and vertical polarization (Jameson and Mueller 1985; Aydin and Giridhar 1992), and 5) errors in the estimation of ϕ_{dp} due to measurement fluctuations (Bringi et al. 1990). These sensitivities limit the physical distance (or accumulated propagation phase shift) over which the correction can be applied successfully (Bringi et al. 1990; Jameson 1991a, 1992).

Based on scattering simulations, Bringi et al. (1990) estimated the correction accuracy for horizontal attenuation and differential attenuation to be within 30% and 35%, respectively, of the mean at C band. This implies that the horizontal reflectivity and differential reflectivity could be estimated to within acceptable error limits, of 1 and 0.3 dB, respectively, if $\phi_{dp} \leq 60°$. Jameson (1991a) clearly demonstrated the sensitivity of the method to variations in the DSD. Jameson (1991a) concluded that the specific differential phase (K_{dp}; range derivative of ϕ_{dp}) could be used to extend the range over which useful measurements of Z_h and Z_{dr} can be obtained at C band. However, because of residual errors in the method, Jameson (1991a) also concluded that the corrected Z_h and Z_{dr} are more suitable for qualitative microphysical applications than quantitative rainfall estimation, except at short ranges (e.g., $<$40 km) or in light rain. Because attenuation is dominated by temperature sensitive molecular absorption at C band for typical drop sizes whereas differential phase shift is not strongly dependent on temperature, the relationship between ϕ_{dp} and α_h (or α_{hv}) is temperature sensitive (Jameson 1992).

Using disdrometer measurements of drop size distributions from Boulder, Colorado, Aydin and Giridhar (1992) developed power law equations for estimating the specific horizontal attenuation (A_h) and the specific differential attenuation (A_{hv}) from K_{dp} at C band. They also noted significant sensitivity to raindrop temperature. They emphasized the need to separate the backscatter differential phase (δ) from the measured, total differential phase (Ψ_{dp}) before calculating K_{dp} (from ϕ_{dp}) because δ can be significant at C band (e.g., Hubbert et al. 1993; Hubbert and Bringi 1995). Using disdrometer measurements of tropical DSDs collected near Darwin, Australia, KCZM and Zrnić et al. (2000) conducted sensitivity analyses of C-band polarimetric variables in tropical rainfall. KCZM showed that the K_{dp}-based estimation of attenuation and differential attenuation is a function of the assumed drop size versus drop shape relationship. Both Zrnić et al. (2000) and KCZM demonstrate that propagation effects are very sensitive to the presence of large drops and assumptions in the analytical parameterization of the large drop tail at C band.

b. Motivation and purpose

Initially, we intended to use published relationships at C band for $A_h(K_{dp})$ and $A_{hv}(K_{dp})$ (e.g., Scarchilli et al. 1993; Gorgucci et al. 1998) to correct Z_h and Z_{dr}, respectively. However, it readily became apparent that choosing a relationship was not a simple matter and required knowledge regarding the DSD, raindrop temperature, and drop shape versus size relationship. Figure 1 depicts a sample of $A_h(K_{dp})$ and $A_{hv}(K_{dp})$ relationships available in the literature for C band (Balakrishnan and Zrnić 1989; Bringi et al. 1990; Jameson 1991a, 1992; Aydin and Giridhar 1992; Tan et al. 1995; Gorgucci et al. 1998; KCZM). For a given value of the specific differential phase, there is *at least a factor of 2* variability in the estimate or A_h and A_{hv} (Fig. 1). As discussed in section 1a, this variability and hence potential error in the estimates of attenuation and differential attenuation are the result of varying temperatures, DSDs, and drop shape relationships utilized in the scattering simulation studies represented by Fig. 1.

As a result, we adapted an *empirical* correction meth-

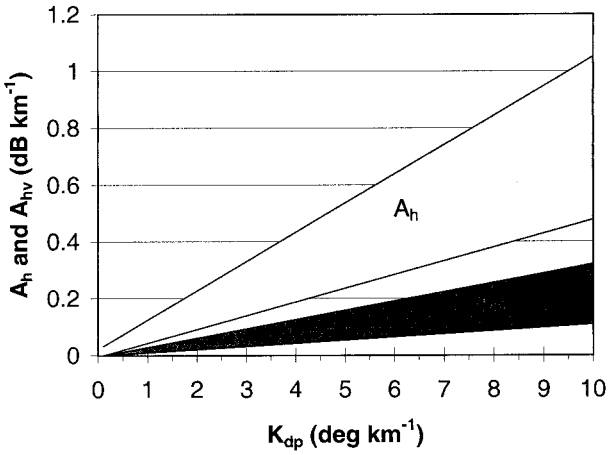

FIG. 1. Plot of specific horizontal attenuation (A_h, dB km^{-1}) and specific differential attenuation (A_{hv}, dB km^{-1}) vs specific differential phase (K_{dp}, ° km^{-1}) in rain as taken from published scattering simulations at C-band (Balakrishnan and Zrnić 1989; Bringi et al. 1990; Jameson 1991a, 1992; Aydin and Giridhar 1992; Tan et al. 1995; Gorgucci et al. 1998; KCZM) that used various drop size distributions and temperatures (−10° to 30°C).

od utilizing the slope of the linear relationship between the observed differential propagation phase (ϕ_{dp}) and the propagation affected Z_h (Z_{dr}) to estimate ''correction factors'' that were then used to estimate α_h (α_{hv}) throughout the radar echo volume. This empirical procedure was first proposed by Ryzhkov and Zrnić (1994) for S-band radar observations. The correction scheme was further refined in Ryzhkov and Zrnić (1995a) and applied in several S-band polarimetric radar studies of midlatitude convection (Ryzhkov and Zrnić 1995a; 1996a,b; Ryzhkov et al. 1997). This method has the advantage of determining the mean linear relationship between ϕ_{dp} and α_h (or α_{hv}) first proposed by Holt (1988) and Bringi et al. (1990) for a particular convective complex without prior knowledge of the appropriate temperature, DSD, or drop shape versus size relationship. As will be demonstrated, this property of the empirical approach eliminates any potential bias and likely mitigates the resultant error in the correction procedure that might have occurred if inappropriate attenuation relationships from Fig. 1 had been chosen instead. In this study, we adapt, improve, and validate the empirical method proposed by Ryzhkov and Zrnić (1995a) at S band for use at C band in the Tropics. An alternate empirical procedure to estimate α_{hv} ray by ray at S band using the negative Z_{dr} in light precipitation behind the attenuation region was proposed recently by Smyth and Illingworth (1998).

The value of α_h (or α_{hv}) for a given ϕ_{dp} increases with both D_0 and D_{max} for a gamma drop-size distribution (Holt 1988; Jameson 1991a; Ryzhkov and Zrnić 1994; Smyth and Illingworth 1998; KCZM 1999). Therefore, the error associated with using a single relationship between ϕ_{dp} and α_h (or α_{hv}) in the correction procedure becomes larger as both median volume diameter and maximum drop diameter (D_0 and D_{max}) increase above mean values. This ''large drop'' effect is particularly important at C band (KCZM). As a result, we have extended the Ryzhkov and Zrnić (1994, 1995a) empirical method to include a simple, large drop correction that extends the conditions over which a useful correction can be applied for the qualitative interpretation of Z_h and Z_{dr} at C band.

2. Mean empirical correction using differential propagation phase

a. Polarization radar data and theoretical basis

During the Maritime Continent Thunderstorm Experiment (MCTEX; Keenan et al. 1994, 1996), observations of tropical rainfall over the Tiwi Islands (Bathurst and Melville Islands, which are centered at about 11.6°S, 130.8°E) were obtained with the Bureau of Meteorology Research Centre C-band (5.3 cm) dual-polarimetric radar (C-pol; Keenan et al. 1998) from 13 November to 10 December 1995. We focus on an intense tropical convective complex with heavy rain that occurred on 28 November 1995. An examination of the complete life cycle of the horizontal and vertical structure of this storm as observed by the C-pol radar can be found in Carey and Rutledge (2000). We supplement these data with additional observations of tropical rainfall on 23 and 27 November 1995.

For C-pol radar specifications and definitions of all observed quantities, see Keenan et al. (1998). We will review herein those definitions required to develop the empirical attenuation correction scheme that utilizes the differential propagation phase. The theoretical basis for attenuation correction schemes using the differential propagation phase (ϕ_{dp}) derives from the finding that specific attenuation (A_h) and specific differential attenuation (A_{hv}) are approximately linearly proportional to the specific differential phase (K_{dp}) at precipitation radar wavelengths (e.g., Bringi et al. 1990):

$$A_h \approx aK_{dp} \tag{1}$$

$$A_{hv} \approx bK_{dp}. \tag{2}$$

By definition, the two-way horizontal attenuation (α_h) and the two-way differential propagation phase (ϕ_{dp}) can be expressed as

$$\alpha_h = 2\int_{r_1}^{r_2} A_h(r)\,dr \tag{3}$$

$$\phi_{dp} = 2\int_{r_1}^{r_2} K_{dp}(r)\,dr. \tag{4}$$

By combining (1), (3), and (4), we find that $\alpha_h = a\phi_{dp}$. This result is then substituted into the definition for the

intrinsic horizontal reflectivity[1] unmodified by propagation effects to obtain

$$Z_h = Z_h^{\text{int}} - \alpha_h = Z_h^{\text{int}} - \alpha\phi_{\text{dp}}, \tag{5}$$

where Z_h is the *measured* horizontal reflectivity. Taking the derivative of (5) with respect to ϕ_{dp}, we obtain the following result (when using finite difference notation):

$$a = \frac{\Delta Z_h^{\text{int}}}{\Delta\phi_{\text{dp}}} - \frac{\Delta Z_h}{\Delta\phi_{\text{dp}}}. \tag{6}$$

After minimizing the *intrinsic* variation of horizontal reflectivity with ϕ_{dp}, the correction factor a is obtained empirically by analyzing the slope of the trend of the observed Z_h with respect to ϕ_{dp}:

$$a \approx -\frac{\Delta Z_h}{\Delta\phi_{\text{dp}}} \tag{7}$$

The two-way differential attenuation (α_{hv}) defined as

$$\alpha_{\text{hv}} = 2\int_{r_1}^{r_2} A_{\text{hv}}(r)\, dr \tag{8}$$

can be combined in a similar fashion with (2) and (4) to obtain the correction coefficient b from actual radar data using the slope of the trend of Z_{dr} with ϕ_{dp}, after minimizing the *intrinsic* variation of Z_{dr} with ϕ_{dp}:

$$b \approx -\frac{\Delta Z_{\text{dr}}}{\Delta\phi_{\text{dp}}}. \tag{9}$$

As shown in the next section, we isolate propagation effects in Z_h and Z_{dr} by restricting the data sample with K_{dp}, ρ_{hv}, and δ thresholds such that intrinsic variations are minimized. The linear slopes in (7) and (9) are then determined using least squares regression on the restricted observations (see section 2c).

Using these empirically derived correction factors, the propagation corrected horizontal reflectivity and differential reflectivity can be obtained from

$$Z_h^{\text{cor}} = Z_h + a\phi_{\text{dp}} \tag{10}$$

$$Z_{\text{dr}}^{\text{cor}} = Z_{\text{dr}} + b\phi_{\text{dp}}, \tag{11}$$

where Z_h and Z_{dr} are the *observed* quantities.

b. Isolating propagation effects

Although the correction method suggested by the theory presented in section 2a is simple in principle, implementation of the technique with real radar data requires careful consideration of the assumptions made in the derivation of (7) and (9). First, regions of spurious polarimetric radar data must be carefully identified and removed. The data processing and quality control procedures for this study are detailed in appendix A. Second, a linear dual-polarimetric radar such as C-pol measures the total differential phase (Ψ_{dp}; Jameson and Mueller 1985),

$$\Psi_{\text{dp}} = \delta + \phi_{\text{dp}} + \phi_0, \tag{12}$$

which must be separated into the backscatter differential phase (δ), differential propagation phase (ϕ_{dp}), and system offset phase (ϕ_0). The system offset phase is a known engineering quantity and can be simply subtracted from Ψ_{dp}. At C band, the backscatter differential phase associated with Mie resonance can be significant, depending on the value of the maximum drop diameter (e.g., Bringi et al. 1990, 1991; Aydin and Giridhar 1992; Hubbert et al. 1993; KCZM). We applied a filtering procedure to remove the contribution of δ to Ψ_{dp} and thereby isolate ϕ_{dp} (e.g., Balakrishnan and Zrnić 1990; Hubbert et al. 1993; Hubbert and Bringi 1995). More details regarding this procedure and the estimation of K_{dp} and its accuracy can be found in appendix A.

Third, we utilized all available multiparameter variables to minimize the intrinsic variation in the Z_h and Z_{dr} samples before determining the correction coefficients in (7) and (9). The goal is to develop a procedure that isolates a particular class of hydrometeors for which the intrinsic (i.e., nonpropagation) variations in Z_h and Z_{dr} are mitigated. In other words, the procedure should minimize the scatter about the slope of Z_h (Z_{dr}) versus ϕ_{dp} [i.e., the first term on the right-hand side of (6)] such that the effects of attenuation (differential attenuation) are clearly represented [i.e., the second term on the right-hand side of (6)]. This goal must be balanced with the requirement to obtain a statistically significant (i.e., sufficiently large) sample of Z_h (Z_{dr}) observations from which a meaningful regression line between Z_h (Z_{dr}) and ϕ_{dp} can be fit.

We utilized specific intervals of K_{dp}, δ, and the correlation coefficient at zero lag between horizontally and vertically polarized electromagnetic waves (ρ_{hv}) in order to isolate a hydrometeor type that is characterized by a limited range of Z_h and Z_{dr}. Ryzhkov and Zrnić (1995a) used S-band radar data characterized by a narrow interval of K_{dp} between 1° and 2° km^{-1}. In order to choose appropriate ranges for C-band observations of K_{dp}, δ, and ρ_{hv} in tropical convection, we simulated radar observables (Z_h, Z_{dr}, K_{dp}, δ, and ρ_{hv}) utilizing DSD data measured with a disdrometer during MCTEX (KCZM) as input to the T-matrix scattering model (Barber and Yeh 1975). The reader is referred to appendix B for specific details and assumptions of the scattering simulations in this study.

From these scattering simulations, we present plots of Z_h and Z_{dr} versus K_{dp} in Figs. 2a and 2b, respectively. As in other scattering simulations of rain at C band (e.g., Bringi et al. 1991; Aydin and Giridhar 1992), Z_h is a logarithmic function of K_{dp}. Note that the range of possible values of Z_h for 1° km^{-1} intervals of K_{dp} is much

[1] The intrinsic reflectivity, Z^{int}, is the reflectivity caused solely by the scattering properties of the hydrometeors in a radar resolution volume.

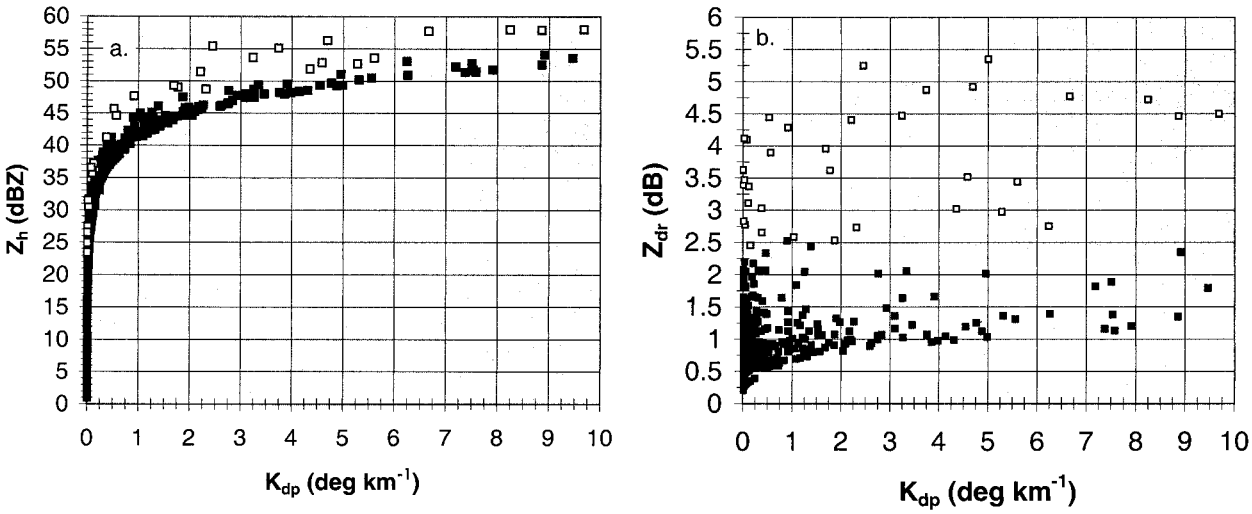

FIG. 2. Plots of (a) horizontal reflectivity (Z_h, dBZ) and (b) differential reflectivity (Z_{dr}, dB) vs the specific differential phase (K_{dp}, $^\circ$ km^{-1}) as obtained from scattering simulations. Solid squares (open squares) are drop size distributions characterized by $\rho_{hv} > 0.97$ and $|\delta| < 1^\circ$ ($\rho_{hv} \leq 0.97$ and $|\delta| \geq 1^\circ$). Details regarding scattering simulations are described in appendix B.

larger at the low end of K_{dp}. This is especially true if we partition the scatterplot in Fig. 2a using ρ_{hv} and δ. The solid (open) squares in Figs. 2a,b are characterized by $\rho_{hv} > 0.97$ and $\delta < 1^\circ$ ($\rho_{hv} \leq 0.97$ and $\delta \geq 1^\circ$). As shown in Bringi et al. (1991) and Aydin and Giridhar (1992), DSDs distinguished by lowered values of ρ_{hv} and large δ have large values of the median volume diameter (D_0) and hence large Z_{dr}. As shown in Fig. 2b, the open (solid) squares are characterized by a mean Z_{dr} of 4 dB (0.7 dB) with a range of 2.5–5.4 dB (0.2–2.6 dB). By removing those DSDs characterized by lowered ρ_{hv} and significant δ (i.e., removing DSDs with large D_0), the scatter of Z_h for a given interval of K_{dp} is significantly reduced. Using this restricted sample, the range of Z_h values for a given K_{dp} interval decreases with increasing K_{dp}. Similarly, the range of Z_{dr} values that have been restricted by $\rho_{hv} > 0.97$ and $\delta < 1^\circ$ also decreases with increasing K_{dp} (Fig. 2b).

Therefore, the use of a 1° km^{-1} interval of K_{dp} above $K_{dp} = 2^\circ$ km^{-1} would minimize the scatter of Z_h and Z_{dr} about ϕ_{dp}. However, the need to minimize the intrinsic scatter must be balanced by the need for a sufficiently large sample to obtain a representative slope described by (7) and (9). These values of K_{dp} would correspond to rain rates in excess of 40 mm h^{-1} at C band (e.g., Carey and Rutledge 2000). Our experience indicates that there are often insufficient grid points characterized by these high rain rates to obtain a good regression. In general, the K_{dp} interval utilized by Ryzhkov and Zrnić (1995a) at S band of 1°–2° km^{-1} is typically a good compromise at C band as well. Inspection of Figs. 2a,b suggest that most values of Z_h (Z_{dr}) should be between 41 and 45 dBZ (0.75 and 1.5 dB).

Unlike Ryzhkov and Zrnić (1995a), K_{dp} thresholds alone did not isolate propagation effects in our study. Because of the increased intrinsic scatter of Z_h and Z_{dr} versus K_{dp} at C band, we found it necessary to apply ρ_{hv} and δ thresholds. The thresholds for ρ_{hv} and δ should be governed by the performance of the radar. Based on the performance of the C-pol radar (Keenan et al. 1998) and a detailed inspection of the data, we chose to restrict the regression using $\rho_{hv} > 0.95$, $|\delta| < 5^\circ$, and $1 \leq K_{dp} \leq 2^\circ$ km^{-1} at grid levels between 0.5 and 2.0 km above ground level (AGL). The effect of varying the regression sample by changing the K_{dp}, ρ_{hv}, δ, and altitude thresholds was explored in sensitivity tests. The above polarimetric and height thresholds provided the most reliable and statistically superior (i.e., low standard error, high coefficient of correlation, and large sample size) least squares fit to the data. A detailed description of the sensitivity tests can be found in Carey (1999).

c. Estimating the mean correction coefficients

Using these thresholds, regression samples for Z_h and Z_{dr} versus ϕ_{dp} are shown in Figs. 3a and 3b, respectively, for 0416 UTC (all times UTC hereafter) on 28 November 1995. In both Figs. 3a and 3b, there is an unmistakably decreasing trend of Z_h and Z_{dr} with ϕ_{dp} due to the effects of horizontal and differential attenuation, respectively. The slope of Z_h (Z_{dr}) versus ϕ_{dp} for the unrestricted sample ($N = 1099$) is -0.071 dB $(^\circ)^{-1}$ (-0.0199 dB $(^\circ)^{-1}$). There is significant scatter of Z_h (4.4 dBZ) and Z_{dr} (0.5 dB) about a least squares fit to the data. This scatter is generally consistent with the simulated data presented in Figs. 2a,b. In addition, there are obvious outliers from the linear fits. For example, the low values of Z_h (<32 dBZ) at relatively low ϕ_{dp} (<20°) in Fig. 3a are inconsistent with the theoretical expectations (cf. Fig. 2a) for Z_h at these ranges of K_{dp}. Enhanced attenuation due to the presence of large raindrops may have caused the presence of these outliers

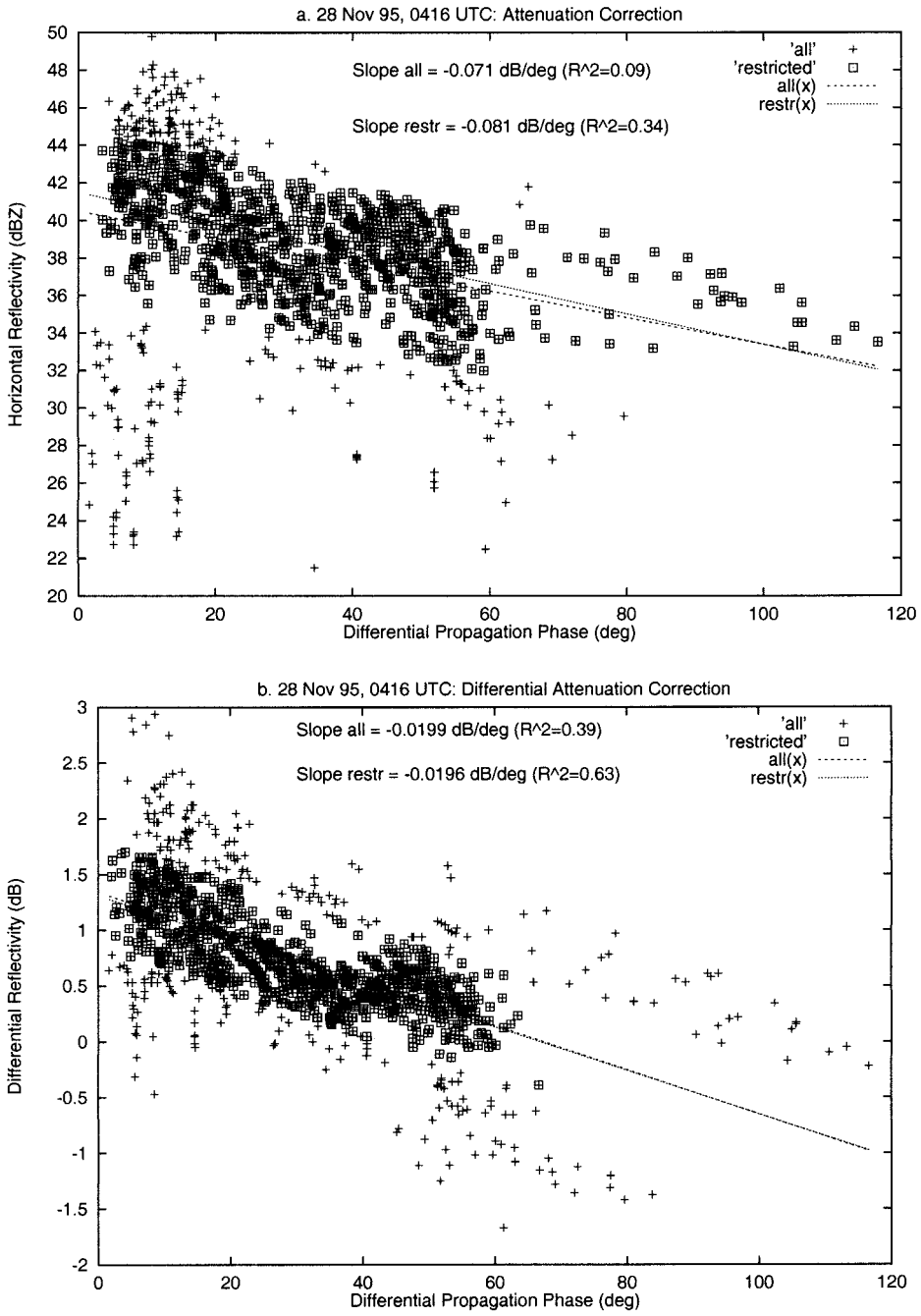

FIG. 3. Least squares linear regression results for (a) horizontal reflectivity (Z_h, dBZ) and (b) differential reflectivity (Z_{dr}, dB) vs the differential propagation phase (ϕ_{dp}, °) taken from 0416 UTC on 28 Nov 1995. The original data sample (+) originated from 0.5 to 2 km and met the following polarimetric radar criteria: $1 < K_{dp} < 2°$ km^{-1}, $\rho_{hv} > 0.95$, and $|\delta| < 5°$. The sample was further restricted by the standard error of the least squares estimate (□). Least square regression slopes for both samples are shown (original sample: short dash; restricted sample: dot).

(cf. sections 3a–c). However, it is also possible that errors in the estimated K_{dp} due to partial beam filling (Ryzhkov and Zrnić 1998a) resulted in the erroneous inclusion of these data points into the regression sample. In Fig. 3b, there are also obvious outliers from the general decreasing trend of Z_{dr} with ϕ_{dp} (e.g., $Z_{dr} < 0.5$ dB and $Z_{dr} > 2.5$ dB for $\phi_{dp} < 15°$). The presence of outliers such as these can seriously bias the inferred correction coefficient.

In order to avoid biasing the mean correction coef-

ficients for each radar volume, the final step in determining the correction coefficients a and b is to eliminate outliers from the linear assumption implicit in the derivation of (7) and (9) using simple statistics. We utilized the standard error of the estimate (S) of Z_h (Z_{dr}) on ϕ_{dp} from a least squares regression line to restrict the sample. We began by removing data outside of $2S$ from the regression line if $\rho < 0.9$.[2] We continued to restrict the sample incrementally by $0.2S$ until $\rho \geq 0.9$ or the data was restricted to within S of the original regression line. Once the restricted sample was obtained, we recalculated the best fit slope to the data using least squares regression. An example of the restricted datasets from 0416 and their associated regression lines are presented in Figs. 3a,b for Z_h versus ϕ_{dp} and Z_{dr} versus ϕ_{dp}, respectively.

Frequently, the slope resulting from the least squares fit to the restricted sample is somewhat different from the original slope. This was the case for Z_h versus ϕ_{dp} at 0416 as shown in Fig. 3a. The final slope of -0.081 dB $(^\circ)^{-1}$ is 14% lower than the original slope of Z_h versus ϕ_{dp}. When a good slope could be determined, the final slope Z_h/ϕ_{dp} differed by no more than 18% from the initial, unrestricted slope. The mean change in Z_h/ϕ_{dp} due to restricting the sample was 9%. Sometimes outliers did not bias the least squares fit and the regression slope did not change significantly after restricting the sample, as for Z_{dr} versus ϕ_{dp} in Fig. 3b. For the entire dataset, retrieved slopes of Z_{dr}/ϕ_{dp} changed by up to 16% with a mean change of 5%. Once the final regression slopes are determined as in Figs. 3a,b, the correction coefficients a and b in (7) and (9) are simply the negative of these two respective slopes.

In order to eliminate significant errors in the propagation corrected Z_h and Z_{dr}, it is important to assess the representativeness of each a and b. The y intercepts from the restricted datasets in Figs. 3a,b should be representative of the propagation-free, intrinsic value of Z_h and Z_{dr}, respectively. The y intercept for Z_h (Z_{dr}) is approximately 42 dBZ (1.3 dB), which is generally consistent with the median value of the scattering simulation results in Fig. 2a (Fig. 2b) for $1 \leq K_{dp} \leq 2^\circ$ km^{-1}. Before utilizing the correction coefficients, we required the coefficient of correlation (ρ), the number of data points in the final regression sample (N), the standard error (S), and the maximum observed ϕ_{dp} to meet the following thresholds: $\rho^2 \geq 0.25$ for a ($\rho^2 \geq 0.6$ for b), $N \geq 200$, $S \leq 5.5$ dBZ for a ($S \leq 0.55$ dB for b), and $\phi_{dp}(\text{max}) \geq 15^\circ$. If all of these conditions were met, then the inferred a and b were used. Otherwise, alternate correction coefficients were determined. If possible, we utilized an interpolation of a and b from adjacent times. As a last resort, we used the median of all successfully determined correction coefficients for the day.

Once correction coefficients a and b were identified for each radar volume, the correction was applied to Z_h and Z_{dr} at each radar gate (or Cartesian grid point) as specified in (10) and (11), respectively. A summary of this propagation correction procedure in the form of a flow-chart can be found in steps 1–4 in Fig. 4. This portion of the algorithm is referred to as the ''mean correction'' because it is equivalent to assuming a single, mean D_0 for the radar volume.

d. Results

Horizontal cross sections of uncorrected Z_h and Z_{dr} at 2 km associated with Figs. 3a,b are presented in Figs. 5a and 5b, respectively. We chose data from 0416 on 28 November 1995 because the convection was widespread and intense. By this time, precipitation had merged on the mesoscale (Carey and Rutledge 2000) with intense convective cores embedded within the complex. Even prior to propagation correction, peak reflectivities and differential reflectivities in these cores ranged from 50 to 55 dBZ and from 2.5 to 4 dB, respectively.

Typically, the effects of attenuation on Z_h are not readily apparent at C band via visual inspection (Fig. 5a). However, differential attenuation visibly decreases the differential reflectivity in range (Fig. 5b). Large areas of negative Z_{dr}, sometimes as low as -2 dB, are apparent down range of convection. Note that the lowest values of Z_{dr} on the back edge of the convection are not necessarily farthest from the radar, nor are they always behind the largest precipitation echo path. Typically, the greatest propagation effects discernible in Z_{dr} are downrange from intense convective cores characterized by large values of reflectivity ($Z_h > 50$ dBZ) and differential reflectivity ($Z_{dr} > 2$ dB), suggesting the presence of large raindrops. These ''large drop cores'' create readily apparent range ''shadows'' of lowered Z_{dr} relative to their immediate surroundings. One example of a shadow in Z_{dr} down range of an intense convective core is highlighted in Figs. 5b, 14a, and 15b.

A horizontal cross section at 2 km of differential propagation phase for 0416 UTC is shown in Fig. 6. Comparison of Figs. 5b and 6 further demonstrates the anticorrelation between ϕ_{dp} and Z_{dr}. As shown earlier in Fig. 3b, increasing values of ϕ_{dp} are generally associated with decreasing Z_{dr} as a result of differential attenuation. Maximum ϕ_{dp} exceeds 120° at this time. Interestingly, this peak occurs less than 50 km in range from the radar. During 28 November 1995, the maximum ϕ_{dp} exceeded 200° several times.

As shown in section 2a, the differential propagation phase is linearly proportional to both the path integrated horizontal and differential attenuation where a and b, respectively, are the constants of proportionality. By multiplying ϕ_{dp} by $a = 0.081$ and $b = 0.0196$ (as de-

[2] The coefficient of correlation (ρ) of a least squares regression line should not be confused with ρ_{hv}, which is the correlation coefficient at zero lag between horizontally and vertically polarized backscattered electromagnetic radiation measured by the radar.

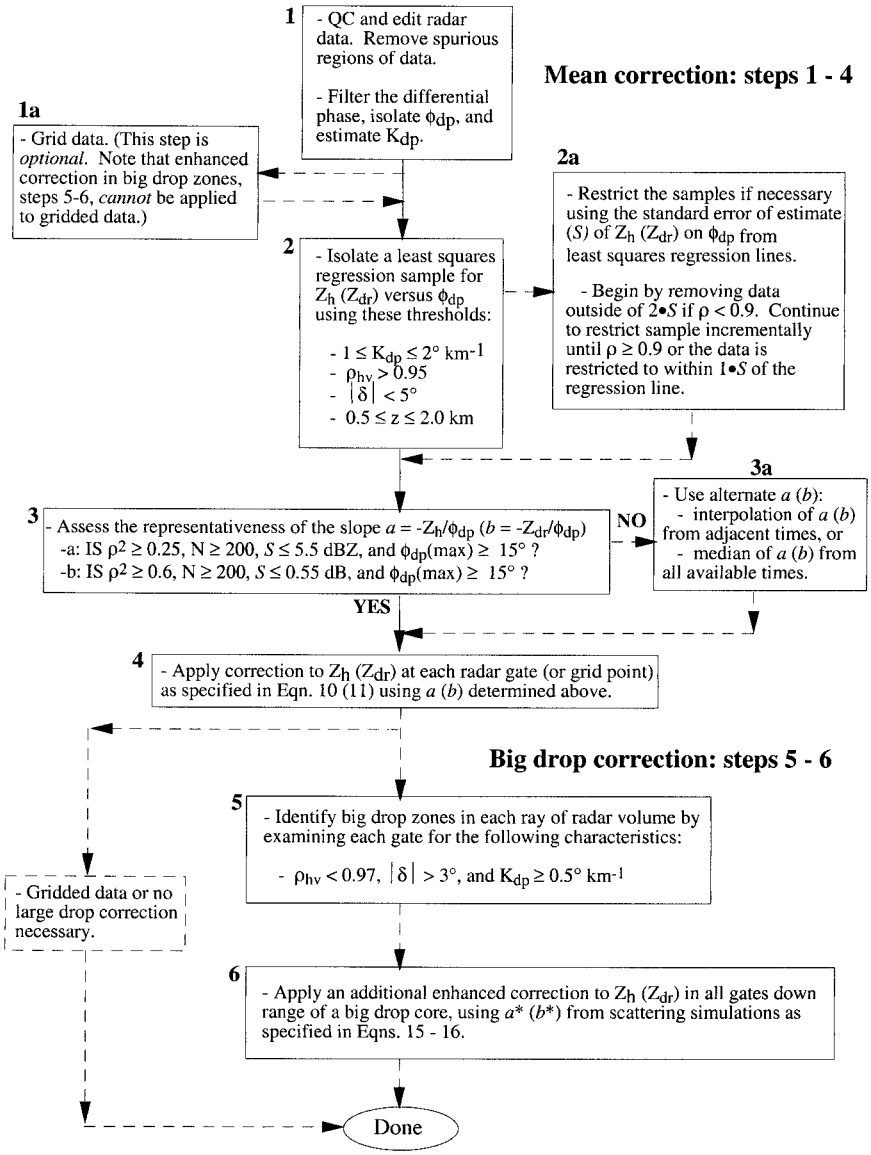

FIG. 4. Flow chart summary of the propagation correction algorithm. Steps 1–4 summarize the mean empirical correction procedure (sections 2a–d) and steps 5–6 depict the big drop correction described in sections 3a–c.

termined in Figs. 3a,b), estimates of α_h and α_{hv} were obtained (Fig. 6). Maximum estimates of α_h and α_{hv} at 2 km exceed 9 and 2 dB, respectively. Approximately 26% of the echo is characterized by significant attenuation ($\alpha_h > 1$ dB) and differential attenuation ($\alpha_{hv} > 0.25$ dB). Five percent of the precipitation echo experienced severe propagation effects (e.g., defined here as $\alpha_h > 4$ dB and $\alpha_{hv} > 1$ dB).

Using the above estimates of propagation effects at 0416 UTC, the corrected Z_h and Z_{dr} were calculated according to (10) and (11) (Figs. 7a and 7b, respectively). As expected, a comparison of Figs. 5a,b to Figs. 7a,b reveals significant differences between observed Z_h/Z_{dr} and propagation corrected Z_h/Z_{dr} in regions of significant ϕ_{dp} (Fig. 6). Most notable is the elimination of most negative values of Z_{dr} in Fig. 7b. Another striking difference is the increased area of precipitation echo characterized by $Z_{dr} > 1$ dB, particularly in the north–south-oriented complex centered on $x = 75$ km and in the cells located 20–50 km to the north-northeast of the radar (Fig. 7b). Similarly, the precipitation echo area characterized by $Z_h > 40$ dBZ also has been substantially increased (Fig. 7a).

To examine the effects of the correction algorithm in three dimensions at 0416 UTC, contoured frequency by altitude diagrams (CFADs; Yuter and Houze 1995) of the uncorrected and corrected Z_h and Z_{dr} are presented in Figs. 8a and 8b, respectively. As expected, the cor-

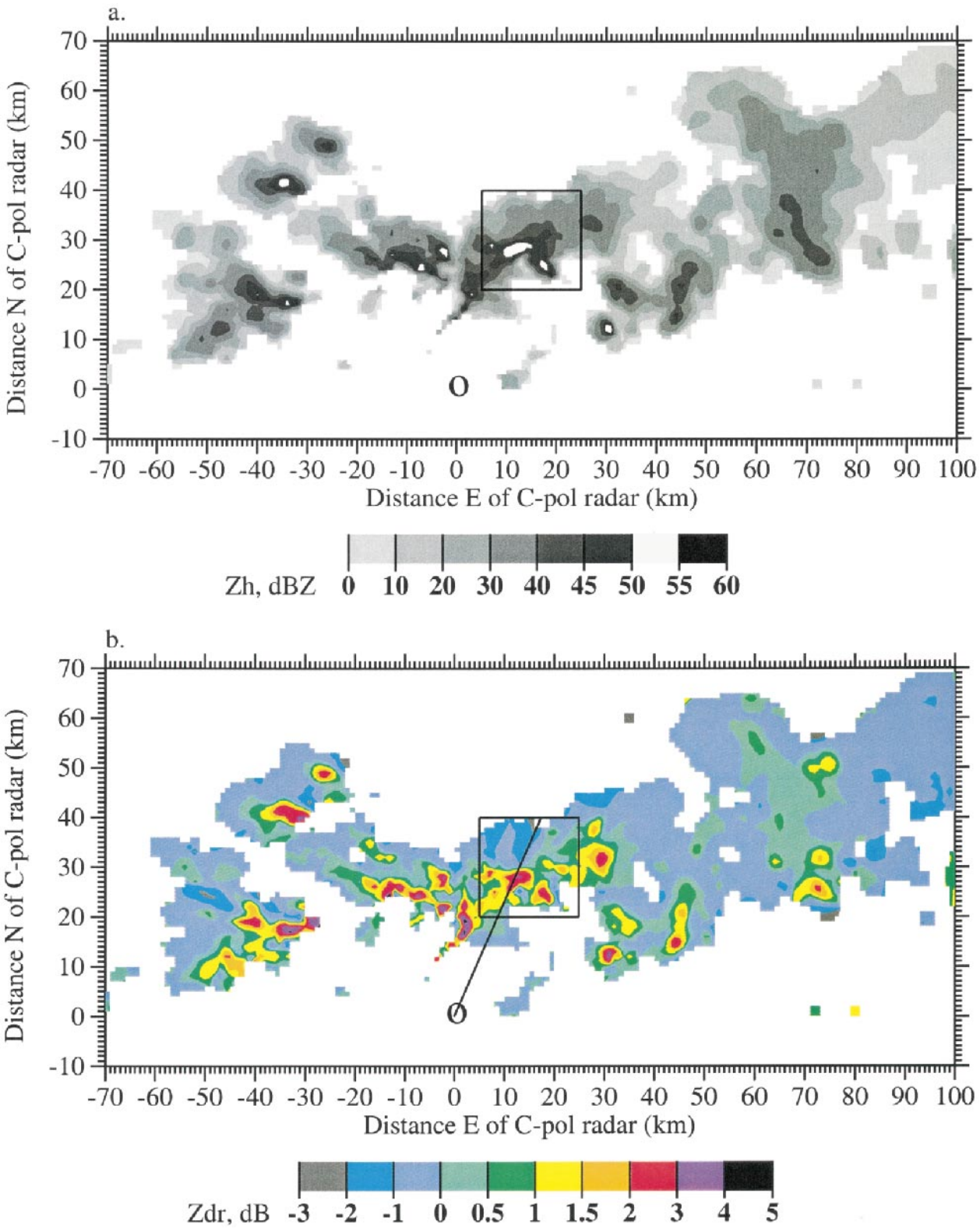

FIG. 5. Horizontal cross section of (a) horizontal reflectivity (Z_h, dBZ, gray shaded) and (b) differential reflectivity (Z_{dr}, dB, color shaded) at 2 km AGL from 0416 UTC on 28 Nov 1995 *before* propagation correction. The position of the C-pol radar is indicated. The box indicates the area covered by Figs. 14a–c. The line in (b) highlights the range ray analyzed in Figs. 15a–c.

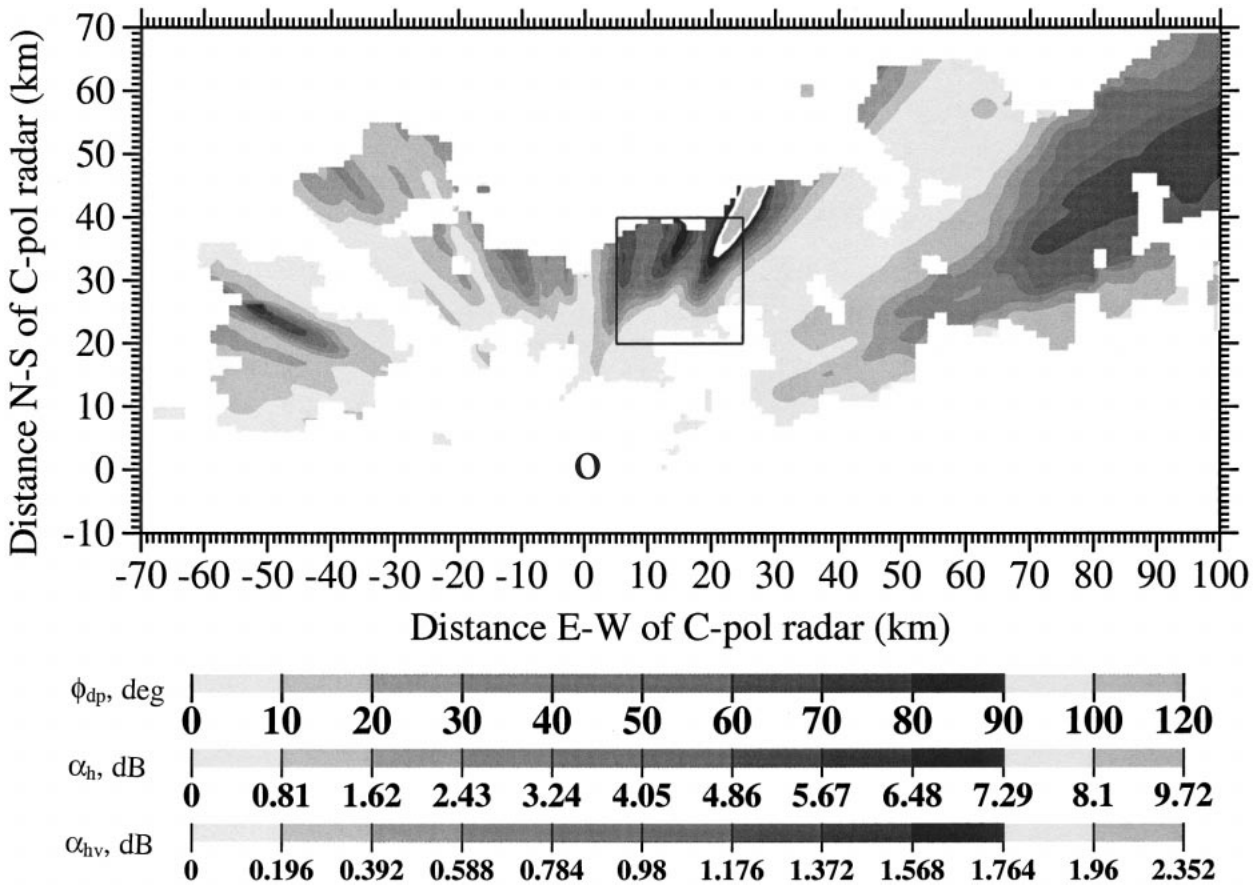

FIG. 6. Horizontal cross section of the differential propagation phase (ϕ_{dp}, °, top shade scale), estimated two-way horizontal attenuation (α_h, dB, middle shade scale), and estimated two-way differential attenuation (α_{hv}, dB, bottom shade scale) at 2 km AGL from 0416 UTC on 28 Nov 1995. The box indicates the area covered by Figs. 14a–c.

rection algorithm primarily affects the lower half of the precipitation echo (<9 km). Below the melting level (5 km), the 1% contour in the Z_h CFAD (Fig. 8a) is shifted approximately 2 dB higher. In other words, 1% of the uncorrected (corrected) echo at a given level is characterized by reflectivities in excess of 44–46 dB*Z* (46–48 dB*Z*). Inspection of Fig. 8b shows that most of the anomalously negative (<-0.5 dB) Z_{dr} present in the original observations were removed by the mean empirical correction procedure. In the uncorrected data, 1% of the Z_{dr} values below the melting level are less than -1.25 dB. In the propagation corrected dataset, less than 0.1% of the data is characterized by $Z_{dr} < -1.25$ dB and the 1% line, on the negative side, ranges from -0.5 to -0.75 dB below the melting level. In addition, the correction algorithm shifted the mode of Z_{dr} higher by 0.5 dB at heights below 7 km AGL. For example, the greater than 10% frequency space for the uncorrected Z_{dr} data at 0.5 km AGL ranges from -0.5 to 0.5 dB. After the correction procedure, the greater than 10% frequency contour for Z_{dr} near the surface brackets the space from 0 to 1 dB. Similar shifts in the mode occurred at all heights below the melting level.

The procedure summarized in steps 1–4 of Fig. 4 was applied to 51 polarimetric radar volumes occurring between 0206 and 0802 UTC on 28 November 1995. Of the 51 polarimetric radar volumes, 61% yielded reliable correction coefficients. Most of the reliable estimates of *a* and *b* were obtained during the mature stage (0330–0630 UTC) of the tropical convection when there were ample propagation effects and widespread convection. During the developing and decaying stage, there were often too few samples with significant attenuation to obtain good regression slopes. For these times, alternate correction coefficients were determined as shown in Fig. 4. We chose this approach, as opposed to not correcting the data, because significant propagation effects (α_h = 1 dB and α_{hv} = 0.25 dB) can occur for just 10°–15° of differential propagation phase, which almost always occurred in at least one range ray somewhere over the islands. Fortunately, when propagation effects became larger and more widespread, the method always yielded a usable estimate of *a* and *b*.

The temporal evolution of the correction coefficients is depicted in Fig. 9. The coefficients *a* and *b* were relatively stable in time before 0502 and after 0514

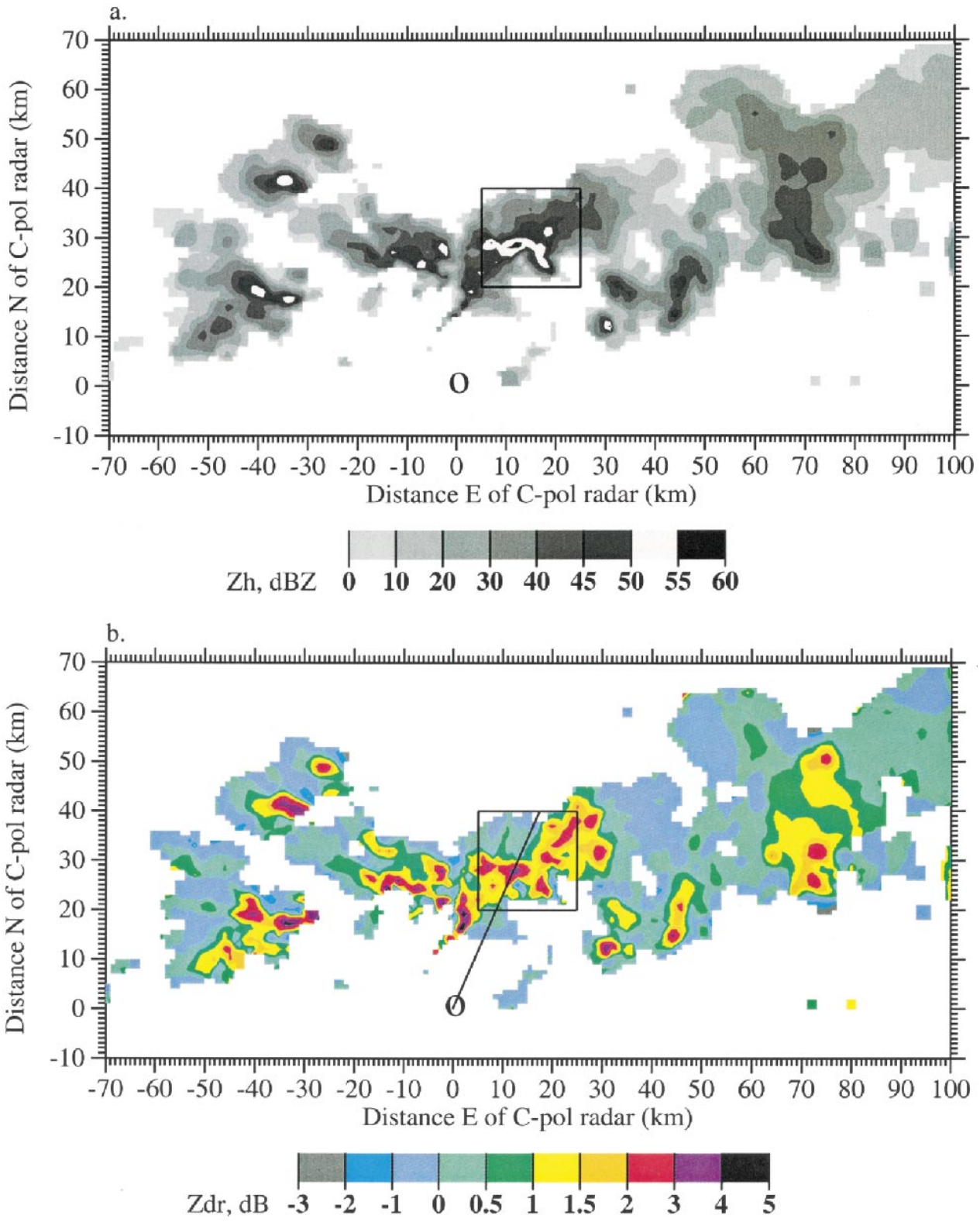

FIG. 7. Same as Fig. 5 except *after* the mean propagation correction procedure summarized in steps 1–4 of Fig. 4 is applied. (a) Horizontal reflectivity (Z_h, dBZ, shaded); (b) differential reflectivity (Z_{dr}, dB, shaded).

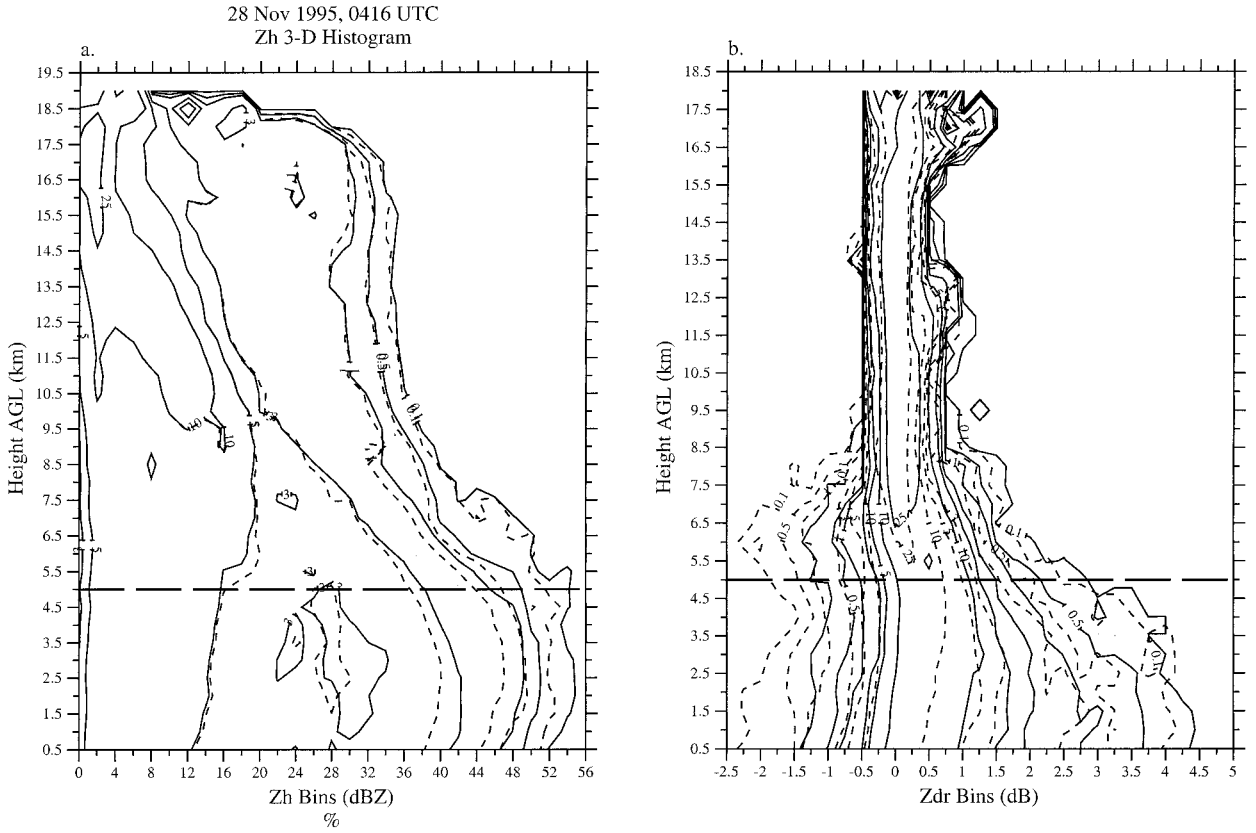

FIG. 8. A CFAD (%) of (a) horizontal reflectivity and (b) differential reflectivity both before and after propagation correction at 0416 UTC on 28 Nov 1995. Before mean propagation correction: dashed line. After mean propagation correction: solid line. The following relative frequencies (%) are contoured: 0.1, 0.5, 1, 3, 5, 10, and 25.

UTC. There was a systematic shift in both coefficients *a* and *b* between 0449 and 0514 UTC. The coefficient *a* increased from 0449 to 0514 UTC while the coefficient *b* decreased. We hypothesize that a systematic shift in the storm wide drop size distribution (DSD) from the developing-to-mature phase (0344–0502 UTC) to the late mature phase (0502–0543 UTC) (see Carey and Rutledge 2000) was responsible for the increase in coefficient *a* and the nearly simultaneous decrease in coefficient *b*. If a change in the storm average DSD was responsible for the systematic and yet opposing temporal behavior of the coefficients *a* and *b*, Fig. 10 suggests that the dominant drop diameter and hence the dominant Z_{dr} of the propagation medium must have decreased. The only portion of the DSD as measured by

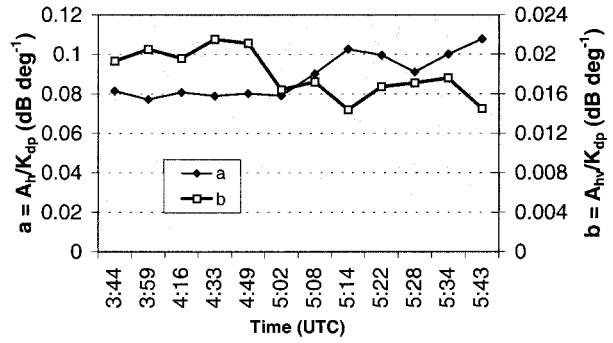

FIG. 9. Temporal evolution of the empirically inferred mean correction coefficients *a* [dB (°)$^{-1}$] and *b* [dB (°)$^{-1}$] from 0344 to 0543 UTC.

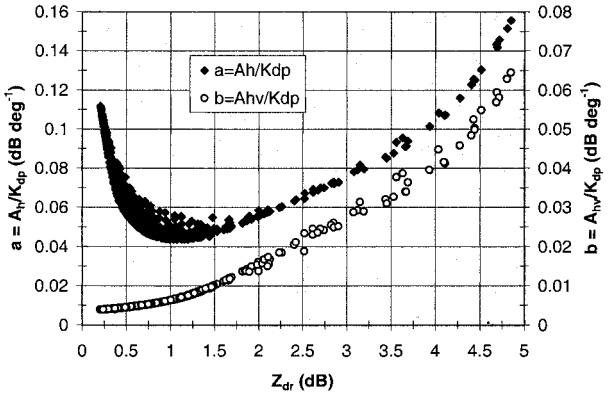

FIG. 10. A plot of the coefficients *a* [dB (°)$^{-1}$] and *b* [dB (°)$^{-1}$] vs Z_{dr} (dB) as derived from scattering simulations described in appendix B.

TABLE 1. Summary of statistics for C-band correction coefficient $a = A_h/K_{dp}$ [dB (°)$^{-1}$] from MCTEX 28 Nov 1995; MCTEX 23, 27, and 28 Nov 1995 combined; and a literature survey.

a [dB (°)$^{-1}$] statistics	28 Nov 1995	23, 27, 28 Nov 1995	Literature*	Literature* $10° < T < 25°C$
Mean	0.0885	0.0932	0.0688	0.0591
Standard error	0.0025	0.0031	0.0032	0.0033
Standard deviation	0.0137	0.0229	0.0153	0.0115
Median	0.0890	0.0901	0.0681	0.0551
Minimum	0.0568	0.0557	0.0426	0.0426
Maximum	0.1113	0.1493	0.1011	0.0789
Count	31	55	23	12

* The literature statistics were derived from the relationships presented in Fig. 1. When necessary, power-based equations were linearized for comparison using a curve-fitting procedure.

Z_{dr} for which a increases and b decreases is below about 1 dB to 1.25 dB (Fig. 10).

To demonstrate a shift in the DSD toward smaller drops later in the storm life cycle, we binned the storm-integrated K_{dp}, which is proportional to specific attenuation and specific differential attenuation, by Z_{dr} at each range gate below 3 km. Toward the end of the mature phase (0543 UTC), the fraction of the storm integrated K_{dp} characterized by $Z_{dr} \leq 1.25$ dB was over 81%, compared to only 51% for 0433 UTC. This shift in the distribution of Z_{dr} strongly suggests a shift in the propagation medium DSD toward smaller drops. In summary, the temporal behavior of the diagnosed correction coefficients was stable and consistent with theory. Systematic and simultaneous changes in the correction coefficients were coincident with systematic changes in convective morphology (i.e., storm maturation) and hence DSD (i.e., decrease in Z_{dr} and D_0). These changes in DSD were then reflected in the expected shift in the correction coefficients (i.e., a increased and b decreased).

Statistics of the inferred correction coefficients a and b for 28 November are given in Tables 1 and 2, respectively. The estimated values of a range from 0.057 to 0.11 dB (°)$^{-1}$. The mean and median of a are both 0.089 dB (°)$^{-1}$. Most inferred values of a range from 0.08 to 0.10 dB(°)$^{-1}$. Retrieved values of b range from 0.012 to 0.030 dB (°)$^{-1}$. The mean and median b are 0.018 and 0.017 dB (°)$^{-1}$, respectively. A majority of estimated values of b range from 0.014 to 0.022 dB (°)$^{-1}$.

For reference, we have supplemented these statistics with results from two other days during MCTEX (23 and 27 November). Statistics for the three combined days are presented in Tables 1 and 2. Note that the 3-day mean and median values for a and b are very similar to those for 28 November (i.e., they vary by less than 15%) and the overall ranges of the correction coefficients are comparable. The stability in the MCTEX correction coefficient statistics presented in Tables 1 and 2 suggest that the method is reliable and that the propagation characteristics (e.g., DSD, temperature, drop shape vs size) vary within a similar range from day to day in tropical convection.

For comparison, statistics for a and b obtained from scattering simulations in the published literature (Fig. 1) are also included in Tables 1 and 2, respectively. These simulations represent a range of temperatures and drop size distributions. Inspection of Tables 1 and 2 demonstrates that these theoretical values of a and b have a similar range as those determined empirically from MCTEX observations. The mean and median of the literature values of a are 25%–30% lower than those determined from MCTEX data. Similarly, the literature simulations of b are about 5%–15% lower than the empirically determined values in the mean. Given the range of conditions simulated in the literature statistics, it is perhaps surprising that the theoretical and empirical

TABLE 2. Summary of statistics for C-band correction coefficient $b = A_{hv}/K_{dp}$ [dB (°)$^{-1}$] from MCTEX 28 Nov 1995; MCTEX 23, 27, and 28 Nov 1995 combined; and a literature survey.

b [dB (°)$^{-1}$] statistics	28 Nov 1995	23, 27, 28 Nov 1995	Literature*	Literature* $10° < T < 25°C$
Mean	0.01819	0.02010	0.01785	0.01617
Standard error	0.00072	0.00057	0.00105	0.00127
Standard deviation	0.00403	0.00435	0.00458	0.00381
Median	0.01720	0.01996	0.01680	0.01570
Minimum	0.0119	0.01190	0.01100	0.01100
Maximum	0.0299	0.03154	0.02810	0.02210
Count	31	59	19	9

* The literature statistics were derived from the relationships presented in Fig. 1. When necessary, power-based equations were linearized for comparison using a curve-fitting procedure.

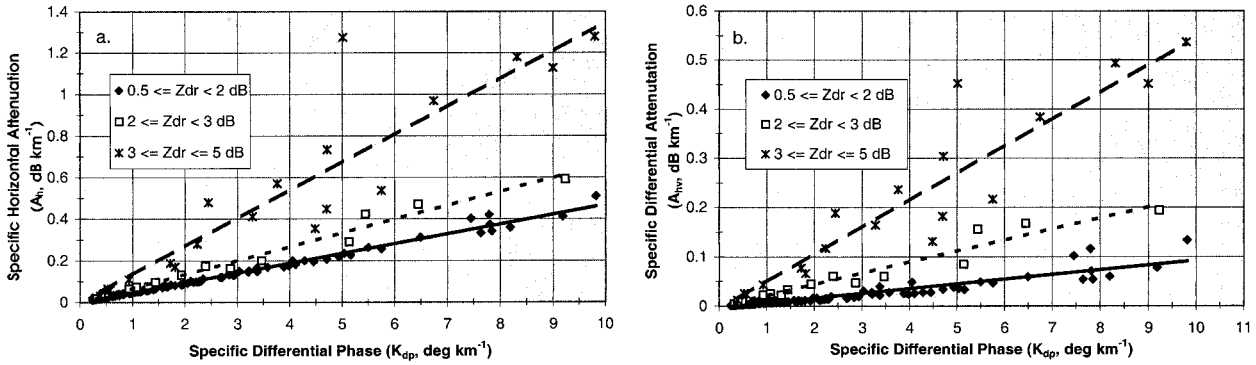

FIG. 11. Scatterplot of (a) specific horizontal attenuation (A_h, dB km^{-1}) and (b) specific differential attenuation (A_{hv}, dB km^{-1}) vs specific differential phase [K_{dp}, (°) km^{-1}] as derived from scattering simulations described in appendix B. The scatterplots are partitioned by the differential reflectivity into three samples as shown. The least squares linear regression line for each group of data partitioned by Z_{dr} is shown. In (a) and (b), the slopes of these lines are equivalent to the coefficients *a* and *b*, respectively, for each data group.

methods obtain reasonably similar estimates of the propagation correction coefficients.

However, closer inspection of the literature scattering simulations suggests more significant discrepancies between theory and empirical results. If we limit literature results to those temperatures that are most representative of the conditions from 0.5 to 2.0 km on 28 November (10°–25°C based on an atmospheric sounding at 0200 UTC), then the literature mean values are reduced to $a = 0.059$ dB (°)$^{-1}$ and $b = 0.0162$ dB (°)$^{-1}$ (Table 1). Note that the maximum values for the coefficients *a* and *b* obtained from the literature survey for $10° \leq T \leq 25$°C are much closer to the *mean* empirical results from MCTEX. In some studies such as Bringi et al. (1990) and Gorgucci et al. (1998), the disagreements with our empirical results are even more serious, particularly for *b*. In these two studies, which utilize similar assumptions regarding the drop-size distribution, the simulated values of *a* (*b*) range from 0.050 to 0.059 dB (°)$^{-1}$ [0.0110 to 0.0157 dB (°)$^{-1}$] for the range of temperatures given above. These values are a factor of 1.6–1.9 smaller than the 3-day empirical means for the coefficients *a* and *b* from MCTEX.

Similar discrepancies between theoretically and experimentally derived estimates of $a = A_h/K_{dp}$ and $b = A_{hv}/K_{dp}$ at S band were reported recently by Ryzhkov and Zrnić (1994, 1995a) and Smyth and Illingworth (1998). Both studies suggest that their higher experimentally inferred values of *a* and *b* were the result of large, oblate raindrops (e.g., $D_0 > 2.5$ mm or $Z_{dr} \geq 2.5$ dB) that were present in their observations but not accounted for in prior theoretical simulations (e.g., Bringi et al. 1990). Both Ryzhkov and Zrnić (1994, 1995a) and Smyth and Illingworth (1998) demonstrate that the coefficients *a* and *b* at S band increase significantly as a function of D_0, particularly for $D_0 > 2.5$ mm. As a result, they suggest that simulations that do not include these large drops tend to underestimate the correction coefficients *a* and *b* under certain microphysical scenarios. As discussed in the next section, we have found a similar dependency of the correction coefficients *a* and *b* on drop size at C band when DSDs including $Z_{dr} > 2$ dB are considered.

3. Large drop correction: A piecewise linear approach

a. Large drop propagation effects

The presence of large raindrops (e.g., $Z_{dr} > 2.5$–3 dB) in tropical convection complicates the correction of propagation effects at C band because the correction coefficients $a = A_h/K_{dp}$ and $b = A_{hv}/K_{dp}$ are an increasing function of Z_{dr}, particularly for $Z_{dr} > 2$ dB, as shown with scattering simulations in Fig. 10. For very large Z_{dr} (e.g., 4 dB), the correction coefficient *a* (*b*) can be a factor of 2 (4) times larger than the coefficient for small to moderate Z_{dr} (e.g., 0.5–2 dB). The correction coefficients *a* and *b* do not vary significantly at these small to moderate values of Z_{dr} and the linear assumptions given by (1) and (2), respectively, are quite accurate as shown in Figs. 11a and 11b. Fortunately, a large majority of the propagation medium in this study was composed of drops characterized by $0.5 < Z_{dr} < 2$ dB (see Fig. C1 in appendix C). As a result, the underlying assumptions of the mean empirical correction method [i.e., (1) and (2)] presented in sections 2a–d are sound in a mean sense, and the standard error of the method for most regions of the storm should fall within the bounds determined by Bringi et al. (1990) and Jameson (1991a, 1992).

When drops with differential reflectivity larger than about 2 dB are considered, the relationship between A_h (A_{hv}) and K_{dp} is better represented by a family of lines in which the slope rapidly increases with Z_{dr} [Fig. 11a (b)]. So, even if the bias in the correction coefficients *a* and *b* is mitigated using the empirical method described in sections 2a–d, the standard error within range and down range of any big drop region could be significantly larger than predicted by Bringi et al. (1990),

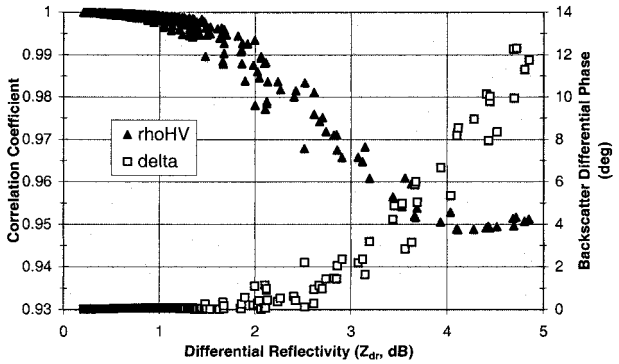

FIG. 12. Scatterplots of the correlation coefficient (ρ_{hv}) and backscatter differential phase [δ, (°)] vs differential reflectivity (Z_{dr}, dB) as derived from the scattering simulations described in appendix B.

because their simulations were truncated at $D_0 = 2.5$ mm. As demonstrated in appendix C, large drop ($Z_{dr} > 3$ dB or $D_0 > 2.5$ mm) precipitation cores occur frequently enough in the Tropics to require an extension to the mean empirical correction method in order to reduce the standard error.

b. Large drop correction method

Obviously, a reliable procedure must be identified to locate large drop zones where enhanced attenuation and differential attenuation can occur. Because differential reflectivity is potentially lowered by differential attenuation, it is not, by itself, a reliable indicator of large drops before correction. At C band, large drop zones can be identified by Mie resonance effects in ρ_{hv} and δ (Bringi et al. 1990, 1991; Aydin and Giridhar 1992; KCZM). As shown with MCTEX scattering simulations (Fig. 12), ρ_{hv} decreases and δ increases significantly with increasing Z_{dr} above 2 dB. For large $Z_{dr} > 3$ dB, these Mie resonance signatures were detectable by the C-pol radar (Keenan et al. 1998; KCZM). After consideration of radar performance and a detailed inspection of the C-pol data, we first identified large drop zones by ''dips'' in ρ_{hv} below 0.97. Because the exact value of δ is a function of maximum drop size (Aydin and Giridhar 1992) and is estimated as a residual from a filtering process (e.g., Hubbert and Bringi 1995), we chose to search for a single perturbation of $|\delta|$ above C-pol's phase noise level of 3° (Keenan et al. 1998) within the region identified by the ρ_{hv} dip. In order to avoid mistaking echoes with low signal-to-noise level as large drops, we also required $K_{dp} > 0.5°$ km^{-1} within the ρ_{hv} dip. If all three of these conditions were met, then the region was declared a large drop zone.

We utilized enhanced correction factors a^* and b^* in those regions defined as ''big drop zones.'' Ideally, a family of correction coefficients that increase in value as Z_{dr} increases from 2 to 5 dB would be utilized (e.g., Figs. 11a,b). However, it was not possible to partition reliably the large drop zones in this manner with C-pol observations because Z_{dr} is affected by differential attenuation and ρ_{hv} and δ cannot be measured with sufficient precision to accomplish this partitioning (Keenan et al. 1998). Therefore, we opted for a simple, first-order correction in big drop zones that utilized a single set of enhanced correction coefficients a^* and b^*.

The empirical technique for determining a^* and b^* typically did not work in large drop zones because 1) the maximum propagation phase shift caused by big drop zones varies from only a couple of degrees to a maximum of 12°, 2) the intrinsic scatter in Z_h and Z_{dr} is often large relative to the attenuation effect, and 3) the large drop cores are relatively rare (1%–6% of echo area) even though their effect can be felt over large areas. As a result, the regression samples from big drop cores were small and had huge scatter and low correlation. Based on comparisons of the scattering simulations (cf. Figs. 10, 11a,b, appendix B) with the mean empirical coefficients a and b (cf. Tables 1 and 2), we chose $a^* = 0.13$ dB (°)$^{-1}$ and $b^* = 0.05$ dB (°)$^{-1}$, which are the mean values of the simulated correction factors for which $\rho_{hv} < 0.97$, $|\delta| > 3°$, and $3 < Z_{dr} < 5$ dB. We were able to confirm these simulated correction factors with a limited application of the regression technique. By combining data from all big drop cores during the most intense period of the convective complex (0416, 0433 UTC), we regressed enhanced correction coefficients of $a^* = 0.16$ dB (°)$^{-1}$ and $b^* = 0.06$ dB (°)$^{-1}$ (which are about 20% higher than simulated). Given the error in the empirical method and the assumptions inherent in our simulations, we believe that the simulated and observed values of a^* and b^* are as close as can be expected. Because the standard errors in the empirical estimates of a^* and b^* were very large, we chose to continue using the simulated values. The use of a single set of correction coefficients for all large drop cores results in a worst-case error of 60%–70% in the estimation of A_h and A_{hv} (Fig. 10). Without enhanced correction factors, the worst case errors associated with the A_h and A_{hv} estimates in large drop cores are 200% and 400%, respectively.

The use of enhanced correction coefficients in large drop zones requires minor modifications to the theoretical basis provided in section 2a. In this instance, a piecewise linear correction approach is utilized. The mean empirical correction factors based on the linear assumption in (1) and (2) are utilized everywhere except in the large drop cores where different slopes are used. We begin by modifying the expression for path integrated horizontal attenuation as a function of range, $\alpha_h(r)$, to include the piecewise linear approximation

$$\alpha_h(r) = 2 \int_0^r a(r')K_{dp}(r')\, dr', \qquad (13)$$

which for the simple case shown in Fig. 13 of a single big drop core occurring from r_1 to r_2 up range (i.e.,

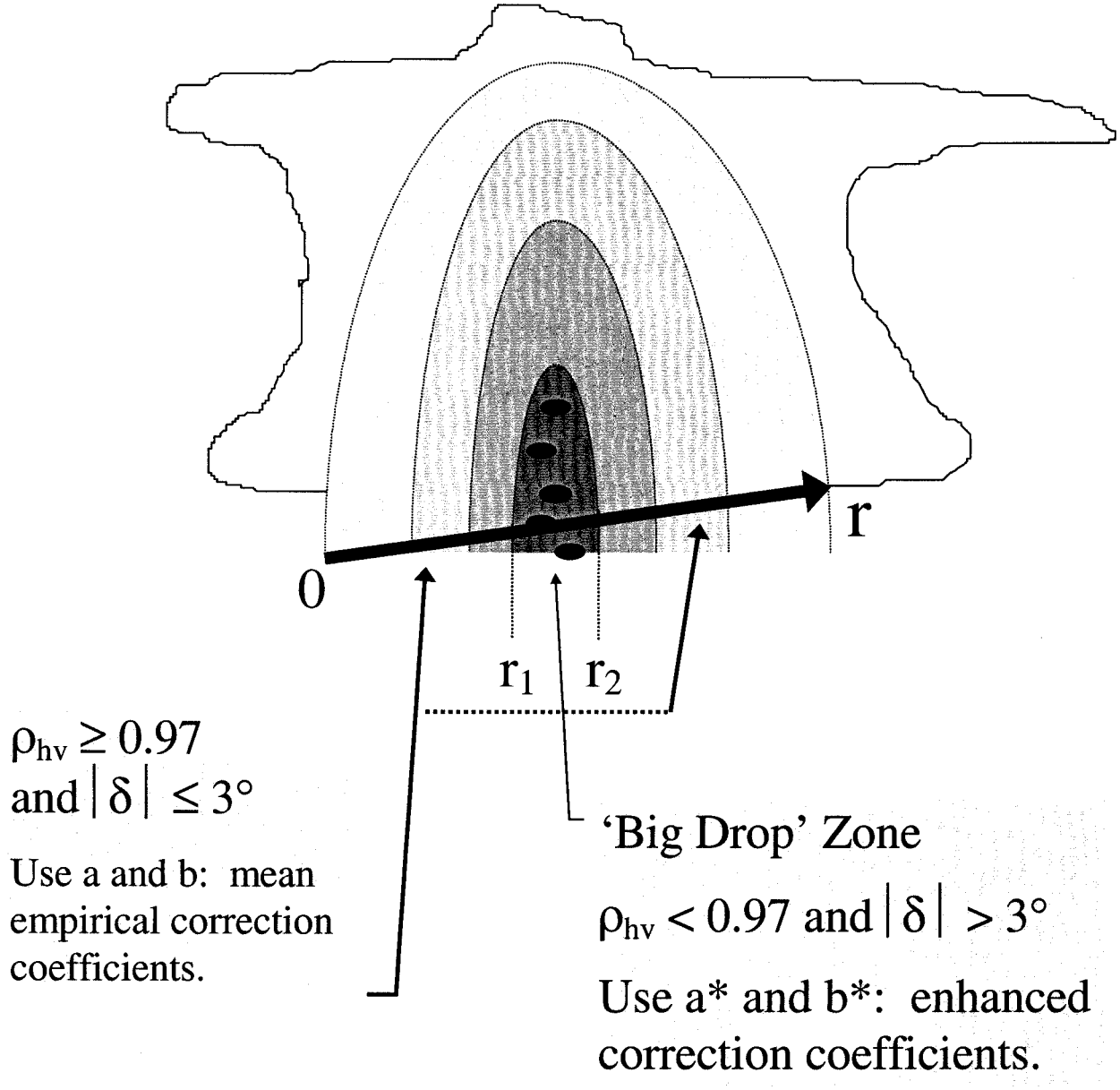

FIG. 13. Illustration of a ray passing through a single big drop zone at ranges r_1 to r_2.

closer to the radar) from the range gate of interest (r) is,

$$\alpha_h(r) = 2a \int_0^{r_1} K_{\rm dp}(r')\, dr' + 2a^* \int_{r_1}^{r_2} K_{\rm dp}(r')\, dr' + 2a \int_{r_2}^{r} K_{\rm dp}(r')\, dr'. \quad (14)$$

By combining (4) and (14) and substituting the result into (5), an expression for the intrinsic or propagation corrected horizontal reflectivity at range r is obtained from

$$Z_h^{\rm cor}(r) = Z_h(r) + a\phi_{\rm dp}(r) + (a^* - a)[\phi_{\rm dp}(r_2) - \phi_{\rm dp}(r_1)], \quad (15)$$

where Z_h is the observed horizontal reflectivity, $\phi_{\rm dp}$ is the differential propagation phase, a is the mean empirical correction factor obtained from the procedure described in sections 2b–d, and a^* is the enhanced correction coefficient. Given the scenario in Fig. 13, a similar approach can be used to derive an expression for the propagation corrected differential reflectivity

$$Z_{\rm dr}^{\rm cor}(r) = Z_{\rm dr}(r) + b\phi_{\rm dp}(r) + (b^* - b)[\phi_{\rm dp}(r_2) - \phi_{\rm dp}(r_1)], \quad (16)$$

where Z_{dr} is the observed differential reflectivity, b is the mean empirical correction factor obtained from the procedure described in sections 2b–d, and b^* is the enhanced correction coefficient. The above derivation can be easily extended to include any number of big drop cores in a given range ray. The complete propagation correction technique utilized in this study, including the big drop correction (steps 5, 6), is summarized in flowchart form in Fig. 4.

c. Results

To demonstrate the enhanced correction procedure in large drop zones, we focus on a region of intense convection at 0416 UTC highlighted by the box in Figs. 5a,b; 6; and 7a,b. An enlarged view of the horizontal and differential reflectivity in this boxed region is presented in Figs. 14a (uncorrected, corresponding to Figs. 5a,b), 14b (mean correction, corresponding to Figs. 7a,b), and 14c (enhanced correction). In Fig. 14a, notice the wedge of negative differential reflectivities (centered on $x = 14$ km and $y = 35$ km) downrange from a core (centered on $x = 13$ km and $y = 28$ km) of large, uncorrected reflectivity (>50 dBZ) and differential reflectivity (2–4 dB). This is a clear example of a big drop precipitation core causing a shadow in Z_{dr} downrange from the radar because of severe differential attenuation.

Based on a visual inspection of Fig. 14b, the mean empirical procedure outlined in sections 2b–d does a reasonably good job correcting the Z_h and Z_{dr}. However, notice the continued presence of the wedge-shaped shadow of lowered Z_{dr} (0–0.5 dB; centered on $x = 14$ km and $y = 34$ km) relative to its surroundings (0.5–1.5 dB) downrange of the big drop core. Typical differential reflectivities in rain for $Z_h > 40$ dBZ are 1–1.5 dB with values as low as 0.5 dB and high as 2.5–4 dB (e.g., Bringi et al. 1991; Aydin and Giridhar 1992; KCZM). The existence of a large area of $Z_{dr} < 0.5$ dB for $Z_h > 40$ dBZ (centered on $x = 14$ km and $y = 33$ km) in Fig. 14b is a clear indicator that some propagation effects remain in Z_{dr} (and therefore probably Z_h too) following the mean correction. The fact that this region exists in a wedge shape downrange from a region of very large Z_h (>55 dBZ) and Z_{dr} (>3 dB), which was shown above to cause enhanced propagation effects, demonstrates the need for an enhanced, big drop correction.

To demonstrate how the big drop correction is applied, range plots passing through a large drop core (Figs. 14a–c) of Z_h and ρ_{hv}, Z_{dr} (and ρ_{hv} repeated), and the various phase measurements (Ψ_{dp}, ϕ_{dp}, K_{dp}, and δ) are presented in Figs. 15a–c, respectively. Using the procedure described above, the big drop zone in the range plots of Figs. 15a–c spans a range of 27.5 to 34 km. Throughout the big drop zone, $|\delta|$ exceeds the threshold of 3° several times (Fig. 15c), ρ_{hv} is below 0.97 (Fig. 15a), and K_{dp} ranges from 0.5° to 5° km^{-1} (Fig. 15c). Note that even prior to correction, the range plots pass through two distinct maxima in Z_h (>50 dBZ) and Z_{dr} (>3 dB) within the defined large drop core. The overall minimum in ρ_{hv} is collocated with both the maximum Z_h (uncorrected and corrected, Fig. 15a) and the maximum Z_{dr} (corrected, Fig. 15b). The combined polarimetric radar signature of large corrected Z_h (50–60 dBZ) and Z_{dr} (2.5–4.5 dB), a minima in ρ_{hv} of 0.88, a maximum $|\delta|$ of 8°, and a peak K_{dp} just under 5° km^{-1} is convincing evidence of a large drop core (e.g., Bringi et al. 1991; Aydin and Giridhar 1992; KCZM).

Clearly, there are severe propagation effects visually evident in raw Z_{dr} as evidenced by the −2 dB value at $r = 40$ km in Fig. 15b. Despite a range of K_{dp} between 1.5 and 4° km^{-1}, the mean corrected Z_{dr} between 33 and 40 km ranges from −0.5 to 0 dB. Results from scattering simulations (Fig. 2b) suggest that the minimum Z_{dr} for the above range of K_{dp} is no less than 0.75 dB. This discrepancy is additional evidence that the mean propagation correction coefficients are insufficient in large drop zones. The enhanced correction procedure results in a final range of Z_{dr} from 0.7 to 1.4 dB at $r = 33$ to 40 km (Fig. 15b). These values of final, enhanced corrected Z_{dr} and estimated K_{dp} are consistent with theoretical expectations (Fig. 2b).

Inspection of Figs. 15a,b reveals that the maximum A_h and A_{hv} within the large drop core reaches 0.64 and 0.25 dB km^{-1}, respectively. The final path integrated attenuation (α_h, Fig. 15a) and differential attenuation (α_{hv}, Fig. 15b) downrange of the big drop zone at $r = 40$ km are 9.3 and 2.9 dB, respectively. The enhanced, big drop correction added 1.9 dB to α_h and 1.1 dB to α_{hv}. After applying the complete propagation correction algorithm, the maximum values of Z_h and Z_{dr} at $r = 32$ km (Figs. 15a,b) are 60 dBZ and 4.8 dB, respectively. While these values are large, equivalent and larger values of Z_h and Z_{dr} were observed in the raw C-pol radar data during MCTEX (Keenan et al. 1998).

The final, enhanced propagation corrected Z_h and Z_{dr} in the boxed region of Figs. 7a,b are shown in Fig. 14c. The wedge of anomalously low Z_{dr} in moderate reflectivity down range of the big drop core is no longer present. The enhanced correction increased Z_{dr} (Z_h) in some areas by 0.25–1 dB (0.5–2 dB) relative to the mean correction. The Z_h/Z_{dr} pairs in Fig. 14c are much more consistent with scattering simulation results (Bringi et al. 1991; Aydin and Giridhar 1992; KCZM) than the uncorrected or mean corrected data. Validation of the complete propagation correction method using cumulative rain gauge data and internal consistency between polarimetric radar observables will be pursued further in the next section (section 4).

After applying the complete propagation correction procedure (steps 1–6) to all polarimetric radar volumes on 28 November 1995, approximately 25% of all range gates containing precipitation echo experienced a significant attenuation correction ($\alpha_h \geq 1$ dB). Similarly, the differential reflectivity was significantly increased

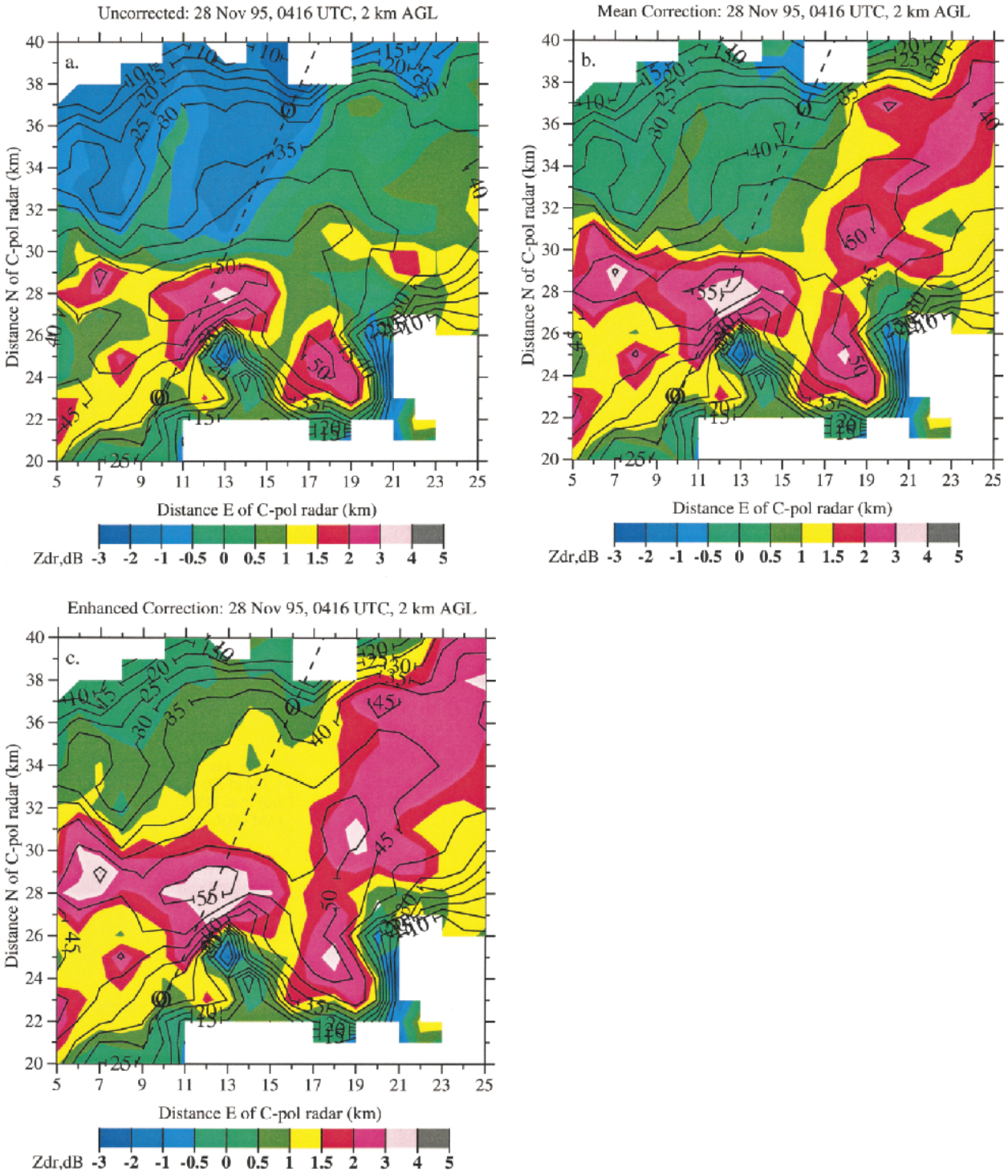

FIG. 14. Horizontal cross section of the differential reflectivity (Z_{dr}, color shaded in dB as shown) and horizontal reflectivity (Z_h, contoured every 5 dBZ starting at 10 dBZ) at 2 km AGL from 0416 UTC on 28 Nov 1995 (a) before any propagation correction, (b) after the mean propagation correction (steps 1–4 in Fig. 4), and (c) after the big drop correction (steps 1–6 in Fig. 4). The dashed line indicates the azimuth analyzed in Figs. 15a–c. Marks along the dashed line approximate the range coverage of Figs. 15a–c. This horizontal cross section zooms in on the boxed area highlighted in Fig. 5.

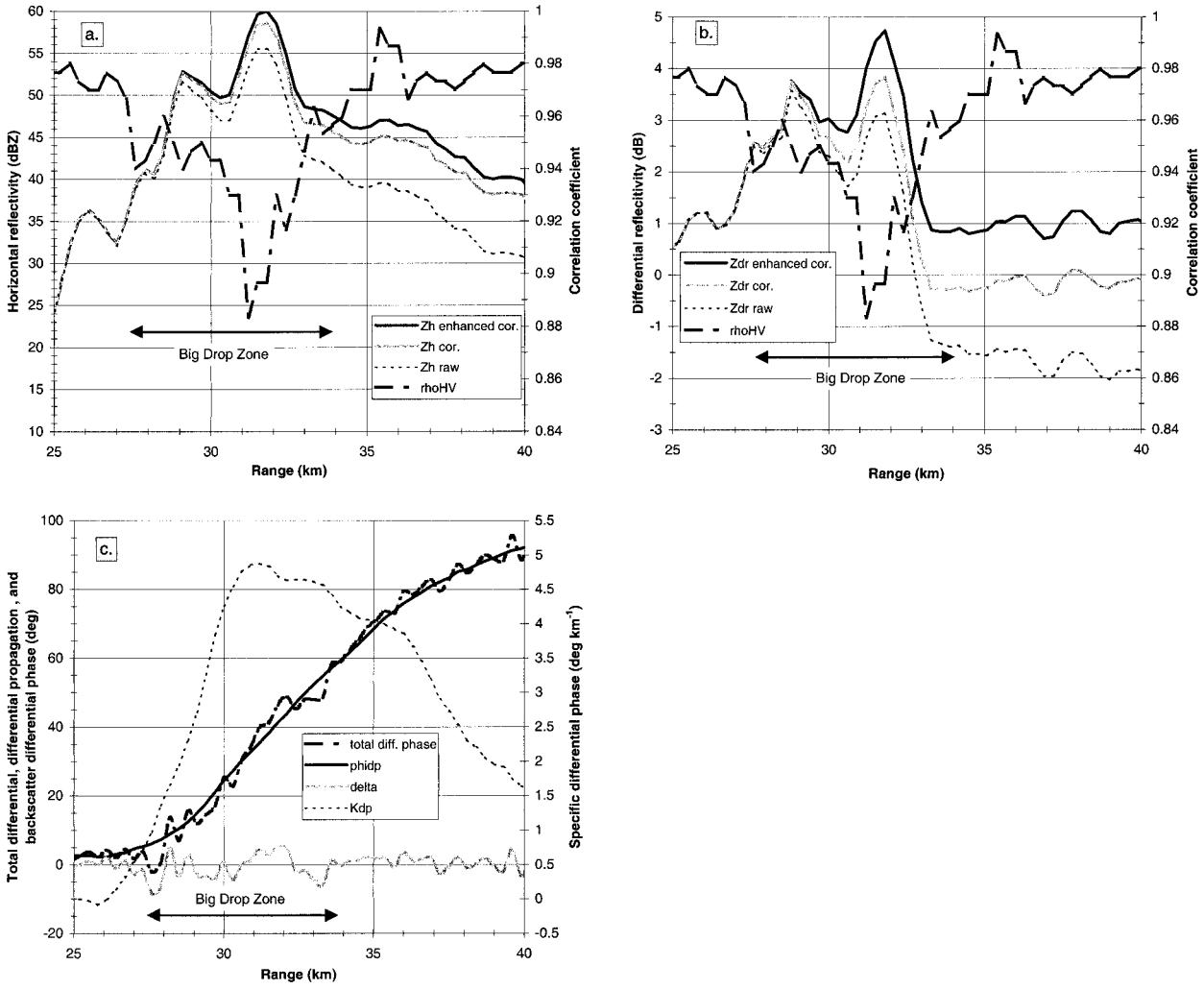

FIG. 15. Range plots of (a) correlation coefficient (ρ_{hv}) and horizontal reflectivity (Z_h, dBZ) before correction (raw), after the mean propagation correction (cor), and after the enhanced correction (enhanced cor.). (b) Correlation coefficient and differential reflectivity (Z_{dr}, dB) before correction (raw), after the mean propagation correction (cor), and after the enhanced correction (enhanced cor.). (c) Total differential phase (Ψ_{dp}, °), propagation differential phase (ϕ_{dp}, °), backscatter differential phase (δ, °), and specific differential phase (K_{dp}, ° km^{-1}). The range plots display ray 387 (azimuth angle = 23.21°, elevation angle = 3.8°) from r = 25 km to r = 40 km. Range resolution is 0.30 km. The big drop zone as defined in the text is highlighted. Refer to Figs. 5b and 14a–c to place this range ray in the context of the entire convective complex.

($\alpha_{hv} \geq 0.25$ dB) about 22% of the time. In about 7% (6%) of the precipitation echo during 28 November 1995, there were massive propagation corrections to Z_h (Z_{dr}) defined as $\alpha_h \geq 5$ dB ($\alpha_{hv} \geq 1$ dB). Clearly, propagation effects at C band in the Tropics are significant and must be corrected before using the data either qualitatively or quantitatively. This premise will be tested further in the next section.

4. Validation

a. Comparison with rain gauge data

Fourteen tipping bucket rain gauges distributed throughout the Tiwi Islands at ranges of 15–88 km from the radar during MCTEX (Keenan et al. 1994) provided an independent dataset from which to judge the efficacy of the above propagation correction algorithm. The time of each bucket tip was logged, each tip representing 0.2 mm of rainfall. The accuracy of the gauge rain rates was typically better than 5%. Quality control of the gauge data included pre- and post-MCTEX rain rate and accumulation calibrations on each gauge.

Our approach was to estimate the cumulative rainfall amount at each gauge while polarimetric data were available (0206–0802 UTC) on 28 November 1995. We chose two independent radar rainfall algorithms to compare to the gauges before and after steps 1–6 (Fig. 4) of the propagation correction algorithm were applied to the C-pol radar data: $R(Z_h)$, and $R(K_{dp}, Z_{dr})$. The equations for these two radar rainfall estimators,

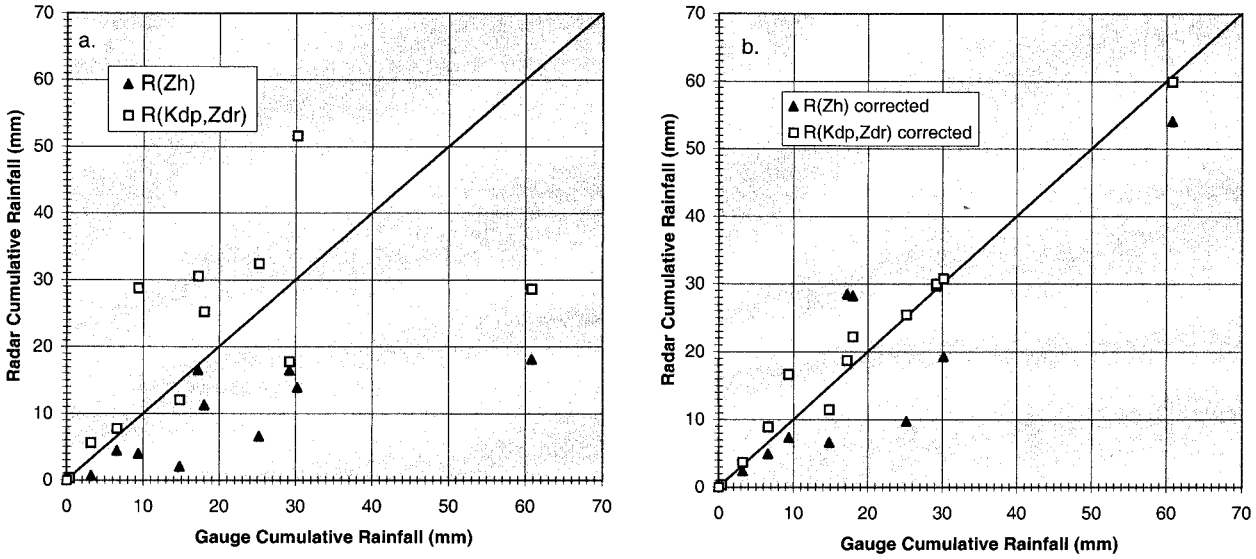

FIG. 16. Scatterplot of the radar cumulative rainfall (mm) [as determined from both $R(Z_h)$ and $R(K_{dp}, Z_{dr})$] vs the gauge cumulative rainfall (mm) for both (a) uncorrected Z_h and Z_{dr} data and (b) propagation-corrected (steps 1–6 in Fig. 4) Z_h and Z_{dr} data.

$$R(Z_h) = 5.865 \times 10^{-3} (Z_h)^{0.862} \quad (17)$$

$$R(K_{dp}, Z_{dr}) = 25.00(K_{dp})^{0.988}(Z_{dr})^{-0.583}, \quad (18)$$

were derived using a curve-fitting procedure on R (mm h^{-1}), Z_h (mm^6 m^{-3}), K_{dp} (° km^{-1}), and Z_{dr} (dB) data from scattering simulations described in appendix B. We compared each gauge rainfall total with the radar cumulative rainfall estimates at the closest 1 km × 1 km grid point.

Comparing the cumulative rainfall amounts over each gauge from $R(Z_h)$, before and after correction, to the associated gauge estimates is intended to assess the performance of the attenuation correction method. Because K_{dp} is unaffected by horizontal or differential attenuation (e.g., Zrnić and Ryzhkov 1996), the relative comparison of the cumulative $R(K_{dp}, Z_{dr})$ rainfall estimates to rain gauge totals before and after correction provides an opportunity to evaluate the results of the differential attenuation correction algorithm. Of course, many other physical and engineering factors enter into the absolute comparison of radar and gauge rainfall estimations (e.g., Zawadzki 1975, 1984). As a result, the use of radar versus gauge rainfall results to substantiate the propagation correction method above is only valid in a *relative* sense. In other words, our only objective was to compare the relative performance of the uncorrected and corrected radar rainfall estimators to the rain gauge totals. A similar approach was taken by Gorgucci et al. (1996). Other studies have focused on the absolute performance of $R(K_{dp}, Z_{dr})$ and $R(Z_h)$ versus rain gauges (e.g., Ryzhkov and Zrnić 1995a; Bolen et al. 1998).

We utilized the normalized bias (NB) and the normalized standard error (NSE) to evaluate the performance of various estimators relative to some reference data or ''truth'' (e.g., rain gauge data). The normalized bias is defined as

$$\text{NB} = \left[\frac{\sum (X_e - X_t)}{n}\right] \Big/ \overline{X}_t \quad (19)$$

and the normalized standard error is defined as

$$\text{NSE} = \left[\sum (X_e - \overline{X}_e - X_t + \overline{X}_t)^2/n\right]^{1/2} \Big/ \overline{X}_t, \quad (20)$$

where X_e is the estimated variable, X_t is the referenced parameter or truth, the overbar indicates a mean, and n is the number of samples.

Results of the polarization radar versus gauge cumulative rainfall comparison before and after the application of the empirical propagation correction method with large drop adjustment are shown in Figs. 16a and 16b, respectively. The NB and NSE for the uncorrected and corrected cumulative $R(Z_h)$ and $R(K_{dp}, Z_{dr})$ relative to the rain gauges are summarized in Tables 3 and 4, respectively.

Before propagation correction, the scatter between the polarization radar and gauge cumulative rainfall amounts is very large (Fig. 16a). This scatter is reflected in very large NSEs of 74% and 83% for uncorrected $R(Z_h)$ and $R(K_{dp}, Z_{dr})$, respectively. As expected, the uncorrected cumulative $R(Z_h)$ significantly underestimated the rain gauge totals (NB = −56%). Since the differential reflectivity is lowered from its intrinsic value by differential attenuation and R is inversely proportional to Z_{dr} [e.g., (18)], the overestimation (NB = +12%) of the uncorrected cumulative $R(K_{dp}, Z_{dr})$ is consistent with theoretical expectations.

After the propagation correction algorithm summarized in Fig. 4 is applied to Z_h and Z_{dr}, the scatter between the radar and gauge cumulative rainfall totals is

TABLE 3. Summary of gauge vs $R(Z_h)$ cumulative rainfall comparison on 28 Nov 1995 from 0206 to 0802 UTC. The differential propagation phase was utilized to correct attenuation effects in Z_h using various correction coefficients (a) as indicated.

	Mean cumulative rainfall (mm)	Normalized bias	Normalized standard error
Gauge	15.36	NA	NA
$R(Z_h)$ no correction	6.76	−56.0%	74.0%
$R(Z_h)$ empirical correction*	13.67	−11.0%	45.1%
$R(Z_h)$ theoretical correction (Gorgucci et al. 1998)**	9.69	−36.9%	59.0%

* Steps 1–6 summarized in Fig. 4 using as from Table 1 and a big drop adjustment ($a^* = 0.130$).
** Correction coefficient ($a = 0.0485$) from simulations of Gorgucci et al. (1998) for $T = 20$°C.

significantly reduced (Fig. 16b). The NSE for the corrected $R(Z_h)$ is reduced to 45%. The NSE for the corrected $R(K_{dp}, Z_{dr})$ is only 16%, compared to 83% for the uncorrected estimator. This represents a fivefold reduction in the $R(K_{dp}, Z_{dr})$ NSE. The NSE of the corrected $R(K_{dp}, Z_{dr})$ is nearly a factor of 3 lower than the corrected NSE of $R(Z_h)$. These NSEs and the superior performance of $R(K_{dp}, Z_{dr})$ as compared with $R(Z_h)$ is consistent with theoretical expectations (Jameson 1991b) and previous experimental results at S band (Ryzhkov and Zrnić 1995b; Bolen et al. 1998). The biases in the corrected, cumulative radar rainfall estimates are also significantly lower, particularly for $R(Z_h)$. The NB for corrected $R(Z_h)$ is reduced by a factor of 5 to −11.0%. For corrected $R(K_{dp}, Z_{dr})$, the NB was reduced by a factor of 2 to 6%. Clearly, the propagation correction algorithm presented above improved the C-band polarization radar estimation of cumulative rainfall during MCTEX.

For comparison, we corrected Z_h and Z_{dr} using ϕ_{dp} and the coefficients a and b derived from the simulations of Gorgucci et al. (1998) (see Tables 3 and 4). Although there was an improvement in the estimation of cumulative rainfall utilizing $R(Z_h)$ in comparison with uncorrected data, the results using the coefficient a from Gorgucci et al. (1998) were not as satisfactory as the empirical algorithm with a large drop adjustment presented in this study. When the Gorgucci et al. (1998) coefficient b was utilized to correct Z_{dr}, the $R(K_{dp}, Z_{dr})$ cumulative rainfall results were actually worse than those using uncorrected Z_{dr} data. In this instance, the Gorgucci et al. (1998) correction of Z_{dr} actually increased the NB by a factor of 4.4 to 53%. Although somewhat counterintuitive, inspection of the radar data provided a reasonable explanation of the result. In several instances, correction of Z_{dr} data with the Gorgucci et al. (1998) coefficient b resulted in an insufficient increase in Z_{dr} from a negative value to a very small, positive value ($0 < Z_{dr} < 0.2$ dB). When Z_{dr} is negative, the $R(K_{dp}, Z_{dr})$ estimator (18) is not defined and does not contribute to the cumulative total. On the other hand, an insufficiently corrected positive value of Z_{dr} near zero combined with a significant value of K_{dp} can resulted in a grossly overestimated rain rate using $R(K_{dp}, Z_{dr})$. As a result, it is possible for a ϕ_{dp}-based propagation correction procedure that utilizes an inappropriately small coefficient b to actually make the $R(K_{dp}, Z_{dr})$ estimator significantly worse when compared with not correcting Z_{dr} at all. This demonstrates the importance of using appropriate values of the coefficients a and b. The empirical method for determining unbiased coefficients described in sections 2a–d is superior to choosing coefficients from the published literature, which vary by at least a factor of 2 (Fig. 1), with limited information regarding DSD and drop temperature.

b. Comparison with scattering simulations

Another approach used to validate the propagation correction algorithm was the internal consistency among polarimetric radar variables. In this case, we examined the behavior of uncorrected and corrected Z_h and Z_{dr} versus K_{dp}, which is unaffected by propagation. As shown in Fig. 2a, scattering simulations predict very regular behavior for intrinsic $Z_h(K_{dp})$, particularly when DSDs characterized by large D_0 are excluded. There is

TABLE 4. Summary of gauge vs $R(K_{dp}, Z_{dr})$ cumulative rainfall comparison on 28 Nov 1995 from 0206 to 0802 UTC. The differential propagation phase was utilized to correct differential attenuation effects in Z_{dr} using various correction coefficients (b) as indicated.

	Mean cumulative rainfall (mm)	Normalized bias	Normalized standard error
Gauges	15.36	NA	NA
$R(K_{dp}, Z_{dr})$ no correction	17.20	+12.0%	82.6%
$R(K_{dp}, Z_{dr})$ empirical correction*	16.31	+6.2%	15.5%
$R(K_{dp}, Z_{dr})$ theoretical correction (Gorgucci et al. 1998)**	23.47	+52.8%	86.7%

* Steps 1–6 summarized in Fig. 4 using bs from Table 2 and a big drop adjustment ($b^* = 0.050$).
** Correction coefficient ($b = 0.0110$) from simulations of Gorgucci et al. (1998) for $T = 20$°C.

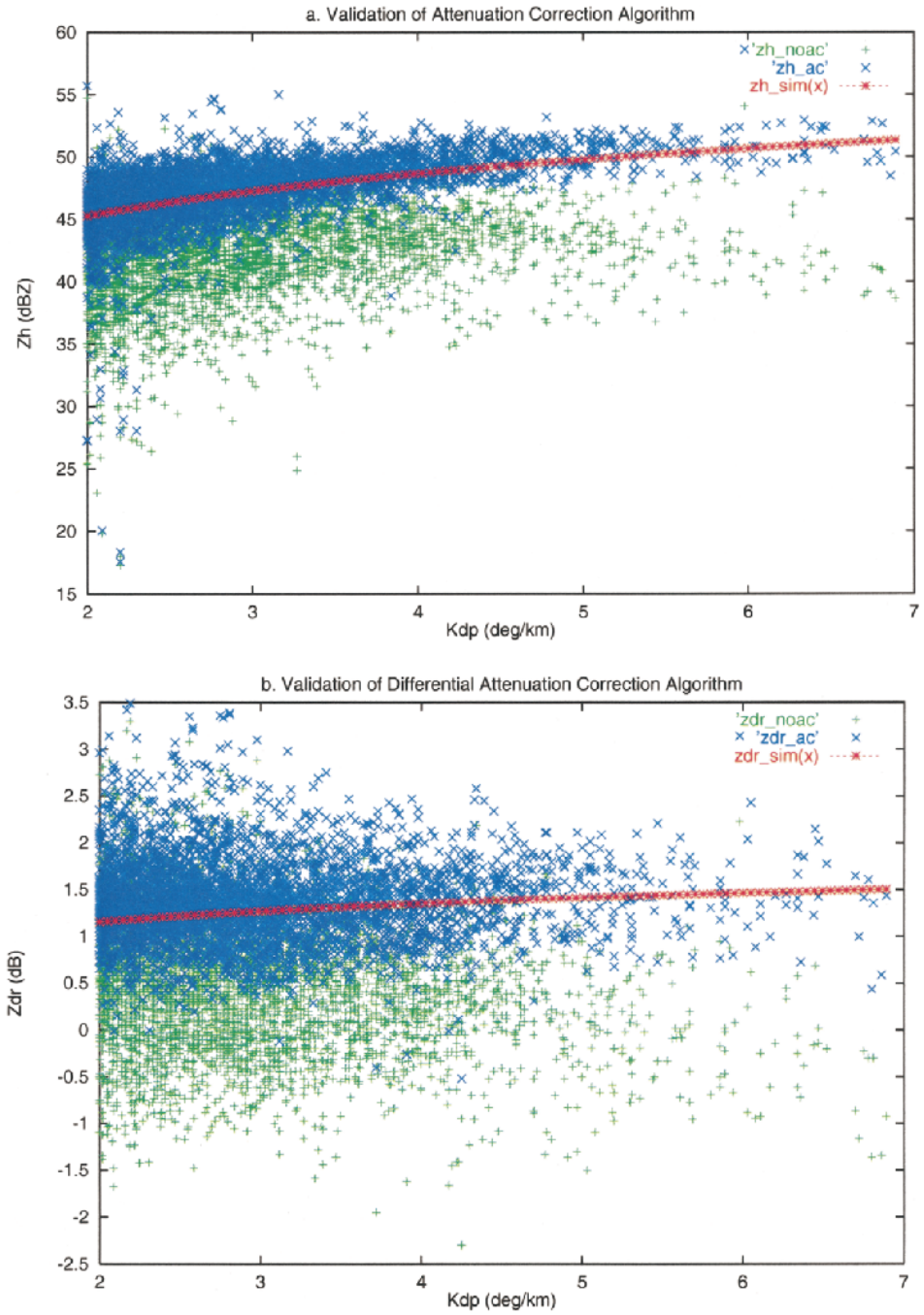

FIG. 17. Scatterplot of C-pol observed (a) horizontal reflectivity (Z_h, dBZ) and (b) differential reflectivity (Z_{dr}, dB) vs the specific differential phase (K_{dp}, ° km^{-1}) both before (green +) and after (blue ×) the propagation correction algorithm summarized in Fig. 4 was implemented. The data are taken from C-pol radar observations at 1–2 km AGL from 0344 to 0543 UTC on 28 Nov 1995. For comparison, the best-fit curves to the scattering simulation results (Figs. 2a,b) are plotted (red *) in (a) and (b), respectively.

significantly more scatter in the intrinsic relationship between Z_{dr} and K_{dp} (Fig. 2b). When large drops are excluded (i.e., consider solid squares only), the scatter is reduced and there is a generally increasing trend in Z_{dr} with K_{dp}. The scatter in both relationships are further reduced when K_{dp} is limited to values in excess of 2° km^{-1}. Therefore, we chose to compare observations of uncorrected and corrected $Z_h(K_{dp})$ and $Z_{dr}(K_{dp})$ to scattering simulation results for which $2 < K_{dp} < 7°$ km^{-1}, $\rho_{hv} \geq 0.97$, and $|\delta| \leq 1°$ (or 3° for C-pol *observations*).

Observations of uncorrected and corrected $Z_h(K_{dp})$ and $Z_{dr}(K_{dp})$ at 1–2 km from 0344 to 0543 UTC on 28 No-

TABLE 5. Validation of propagation correction method using internal consistency among the polarimetric variables. Comparison of C-pol observations (for $2^\circ < K_{dp} < 7^\circ$ km^{-1} at 1–2 km AGL from 0344 to 0543 UTC on 28 Nov 1995) of Z_h (K_{dp}) and Z_{dr}(K_{dp}) both before and after correction to scattering simulation (assumptions of scattering simulation discussed in appendix B) results.

	Mean	Bias (normalized bias)	Standard error (normalized standard error)
Z_h			
Scattering simulation	47.02 dBZ	NA	0.78 dBZ (1.6%)
No attenuation correction	42.63 dBZ	−4.40 dBZ (−9.4%)	3.46 dBZ (7.4%)
Attenuation correction	47.36 dBZ	0.34 dBZ (0.7%)	2.07 dBZ (4.4%)
Z_{dr}			
Scattering simulation	1.26 dB	NA	0.44 dB (34.9%)
No differential attenuation correction	0.49 dB	−0.77 dB (−61.2%)	0.66 dB (52.4%)
Differential attenuation correction	1.37 dB	0.11 dB (8.7%)	0.43 dB (34.1%)

vember 1995 are presented in Figs. 17a and 17b, respectively, along with curve fits to the appropriate simulation results (solid squares) shown in Figs. 2a,b. As expected, the uncorrected observations of Z_h and Z_{dr} significantly underestimate the theoretical expectation represented by the simulation curves. The bias in the uncorrected Z_h (Z_{dr}) observations for this range of K_{dp} is −4.4 dB (−0.8 dB). In addition, the standard error of the uncorrected observations is considerably larger than the simulation results. For example, the standard error in the uncorrected $Z_h(K_{dp})$ and $Z_{dr}(K_{dp})$ scatterplots is 3.5 dBZ and 0.7 dB, respectively. Note that our scattering simulations do not include the effects of measurement error. Typical errors, which are independent of propagation effects, for C-pol observations of Z_h and Z_{dr} are 1 dBZ and 0.25 dB, respectively (Keenan et al. 1998). A summary of the biases and standard errors resulting from the validation exercise are given in Table 5.

The propagation correction procedure nearly removed the significant observational biases in both the $Z_h(K_{dp})$ and $Z_{dr}(K_{dp})$ scatterplots with respect to theory (Figs. 17a and 17b, respectively). After correction, the biases in $Z_h(K_{dp})$ and $Z_{dr}(K_{dp})$ decreased to 0.34 dBZ and 0.11 dB, respectively. These order-of-magnitude reductions in the biases represent a substantial improvement over the uncorrected results. In addition, the scatter in both relationships was reduced considerably and is now more consistent with the scattering simulations (cf. Figs. 17a,b; 2a,b). For example, the standard errors for both $Z_h(K_{dp})$ and $Z_{dr}(K_{dp})$ were reduced by 35%–40% to 2 dBZ and 0.4 dB, respectively.

In order to test the point-to-point consistency of the corrected Z_h and Z_{dr}, we compared the estimated $K_{dp}(Z_h, Z_{dr})$ directly with the measured K_{dp} as in the $K_{dp}/Z_{dr}/Z_h$ calibration technique (e.g., Tan et al. 1995). For $0.5 \le Z_{dr} \le 1.5$ dB, we fit a power-law equation

$$K_{dp}/Z_h = 6 \times 10^{-5} (Z_{dr})^{-0.636} \quad [(^\circ \text{ km}^{-1})\ (\text{mm}^6\ \text{m}^{-3})^{-1}] \tag{21}$$

to our simulated MCTEX radar data to estimate K_{dp}/Z_h from Z_{dr}. We then utilized (21) to estimate K_{dp} from the measured Z_h and Z_{dr} both before and after the propagation correction procedure. Before the correction procedure, the best-fit linear slope for pairs of (K_{dp} measured, K_{dp} estimated) was 0.67, suggesting that the estimated K_{dp} was lower than measured. After correction, the best-fit linear slope was 0.99 with 80% of the variance explained. In estimating K_{dp}, the uncorrected Z_h and Z_{dr} produced a bias (normalized) of -0.2° km^{-1} (−25%). Our propagation correction algorithm decreased the bias by more than a factor of 2; the corrected Z_h and Z_{dr} resulted in a bias (normalized) of only -0.08° km^{-1} (−10%) in the estimated K_{dp}.

Clearly, the uncorrected Z_h and Z_{dr} observations are ill suited for quantitative use (i.e., rainfall estimation as shown above) or even qualitative use (i.e., hydrometeor identification). As shown in Carey and Rutledge (2000), the relationships among Z_h, Z_{dr}, and K_{dp} are used to differentiate between rainfall and precipitation-sized ice and provide a rough estimate of their amounts. In addition to corrupting the estimation of rainfall (section 4a), these huge biases and standard errors in uncorrected Z_h and Z_{dr} could result in widespread, incorrect hydrometeor identifications and undefined results. Fortunately, the propagation correction algorithm described in sections 2 and 3 substantially reduces both the bias and the standard error in Z_h and Z_{dr} (Table 5; Figs. 17a,b) relative to theoretical expectations. In Carey and Rutledge (2000), we demonstrate that the propagation-corrected Z_h and Z_{dr} are of sufficient quality to differentiate between raindrops and precipitation-sized ice particles in the large majority of convective situations.

5. Summary and conclusions

Before interpretation or quantitative analysis of C-band polarimetric radar data can begin, propagation effects must be identified and removed. In particular, the horizontal (differential) reflectivity must be corrected for the deleterious effects of horizontal (differential) attenuation. In this study, we utilized the differential propagation phase to estimate both the horizontal

and differential attenuation at C band. This phase-based approach has several advantages over traditional power-based algorithms. The specific differential phase 1) is immune to power calibration errors (e.g., Zrnić and Ryzhkov 1996), 2) is not adversely affected by attenuation (e.g., Zrnić and Ryzhkov 1996), and yet 3) is approximately linearly proportional to both the specific horizontal and differential attenuation (e.g., Bringi et al. 1990).

The relationship between A_h or A_{hv} and K_{dp} is dependent on temperature, DSD, and the drop shape versus size relationship (e.g., Bringi et al. 1990; Jameson 1991a, 1992; KCZM). As a result, the calculated values of A_h and A_{hv} for a specific K_{dp} vary by a factor of 2 or more for relevant precipitation characteristics in published scattering simulations (see Fig. 1). Without specific information on DSD, temperature, and drop shape throughout each radar echo volume, an unbiased estimate of $a = A_h/K_{dp}$ and $b = A_{hv}/K_{dp}$ cannot be chosen from these published simulations. Therefore, we adapted and modified the empirical approach of Ryzhkov and Zrnić (1995a) to estimate unbiased correction coefficients a and b for each radar volume.

The coefficients a and b are estimated from the observed decreasing trends of Z_h and Z_{dr}, respectively, with ϕ_{dp}. A least squares regression technique was applied to observed data to estimate the linear slope of this trend. The theoretical basis for this procedure was reviewed and the regression method was presented and tested using C-pol radar observations taken during MCTEX. In order to extract the effects of propagation, the intrinsic variations in Z_h and Z_{dr} must be minimized. As in Ryzhkov and Zrnić (1995a), we utilized a specific range of K_{dp} to mitigate intrinsic differences in Z_h and Z_{dr}. However, we found it also necessary to use ρ_{hv}, δ, and height to restrict the sample from which a and b were estimated. These polarimetric radar thresholds were chosen using scattering simulation results as a guide. Tropical drop-size distributions observed during MCTEX were used as input for these scattering simulations. Statistical procedures to minimize biases in the inferred coefficients a and b were proposed and demonstrated. Last, a mechanism to test the representativeness of the estimated correction coefficients was presented.

During the mature phase of a tropical convective system on 28 November 1995, the empirical regression technique reliably produced statistically acceptable correction coefficients. The temporal behavior of the diagnosed correction coefficients was stable and consistent with theory. Systematic and simultaneous changes in the correction coefficients were coincident with systematic changes in convective morphology (i.e., storm maturation) and hence DSD (i.e., decrease in Z_{dr} and D_0). These changes in DSD were then reflected in the expected shift in the correction coefficients (i.e., a increased and b decreased).

The range of empirically estimated coefficients was generally consistent with theoretical expectations. However, the coefficients a and b determined from prior scattering simulations tended to be 10%–30% lower than the empirical results from MCTEX. When considering appropriate temperatures ($10° < T < 25$°C) for tropical rainfall at 0.5 to 2 km AGL, the empirically inferred coefficients from MCTEX are 1.5–2 times larger than prior scattering simulations. This significant discrepancy between observations and theory at C band in the Tropics is similar to midlatitude results at S band by Ryzhkov and Zrnić (1994, 1995a) and Smyth and Illingworth (1998).

Using scattering simulations, we demonstrated that a (A_h/K_{dp}) and b (A_{hv}/K_{dp}) are sensitive functions of the drop size if large raindrops are present. For small to moderate values of Z_{dr} (0.5–2 dB), the coefficients a and b are relatively insensitive to drop size. For $Z_{dr} > 2$ dB, the coefficients a and b increase rapidly as a function of Z_{dr}. As a result, the value of a (b) for large drops (e.g., $Z_{dr} = 4$ dB) is a factor of 2 (4) times larger than the coefficient for small- to moderate-sized drops. There are two implications for this large drop sensitivity: 1) as also determined by Ryzhkov and Zrnic (1994, 1995a) and Smyth and Illingworth (1998), the presence of large drops can bias the mean coefficients higher than prior scattering simulations (e.g., Bringi et al. 1990); and 2) the standard error for corrected Z_h and Z_{dr} in precipitation downrange from large drop cores can be significantly larger than predicted by Bringi et al. (1990) if the mean coefficients are utilized. Because in situ and radar observations during MCTEX confirmed the presence of large raindrops in tropical convection, these effects were deemed to be significant. The mean empirical method automatically eliminates any bias caused by the presence of large drops because no assumptions regarding DSD are made. Without some extension to this procedure however, the error down range from big drop cores was unacceptably large.

To minimize this error, we proposed the use of enhanced correction coefficients in so-called big drop zones. The enhanced correction coefficients a^* and b^* were determined from scattering simulations of large drops and were confirmed by a limited application of the empirical regression technique in large drop zones. To locate large drop zones ($D_0 > 2.5$ mm) in the observed C-band data, we searched for dips in ρ_{hv} accompanied by significant perturbations in δ caused by Mie resonance effects. The method was demonstrated on observations of intense MCTEX convection containing a clear-cut example of enhanced propagation effects down range from big drop cores. The big drop correction significantly improved the qualitative results of the correction procedure.

To validate the overall propagation correction algorithm utilizing the differential propagation phase, cumulative rain gauge amounts were compared with cumulative radar rainfall estimates using $R(Z_h)$ and $R(K_{dp}, Z_{dr})$ before and after correction. The correction procedure significantly reduced both the bias and stan-

dard error of both cumulative radar rainfall estimates to within expected ranges given typical measurement errors other than propagation. To verify further the procedure, we compared the behavior of Z_h and Z_{dr} with K_{dp} both before and after correction to theoretical expectations generated with scattering simulations. The uncorrected $Z_h(K_{dp})$ and $Z_{dr}(K_{dp})$ significantly underestimated the simulation results. The correction procedure reduced these negative biases by nearly an order of magnitude and substantially reduced the standard error of the observations relative to scattering simulations. Finally, we compared the estimated $K_{dp}(Z_h, Z_{dr})$ to the measured K_{dp}. The propagation correction algorithm reduced the bias in the estimated mean $K_{dp}(Z_h, Z_{dr})$ by a factor of 2.5 to only -10% (-0.08° km^{-1}). This validation result provides additional confidence in the mutual consistency between the corrected Z_h and Z_{dr}.

Given these validation results, we proceeded to qualitatively interpret and quantitatively analyze the propagation corrected Z_h and Z_{dr} with confidence in Carey and Rutledge (2000). The repeated correlation between radar-inferred precipitation characteristics and cloud electrification and lightning demonstrated in Carey and Rutledge (2000) provide additional indirect support for our propagation correction algorithm. Because the procedure was only tested on three case studies during MCTEX, continued testing of the procedure on other case studies and with other C-band radars would be beneficial. Moreover, a long-term, quantitative study in an operational setting on a large amount of data would be required to determine if the algorithm could be implemented reliably on an operational radar.

Because many radar meteorologists utilize precipitation radar wavelengths other than C band (e.g., S band and X band), a few words regarding the application of this correction algorithm to other wavelengths is warranted. Given the modeling studies of Bringi et al. (1990) and Jameson (1991a, 1992) and the empirical results of Ryzhkov and Zrnić (1995a), we are confident that the mean correction coefficients can be determined at X band and S band using empirical regression techniques similar to those used in this study. The correction technique is sensitive to fluctuations in the DSD at both S band (Bringi et al. 1990) and X band (Bringi et al. 1990; Jameson 1991a). Therefore a big drop correction is warranted at these wavelengths too. At X band, the backscatter differential phase is large and measurable in large drop cores. Assuming the iterative filtering technique of Hubbert and Bringi (1995) can accurately estimate significant values of the backscatter phase (e.g., $\delta > 3^\circ$) at X band, large drop cores should be identifiable and a large drop correction could be applied. Given typical radar performance, ρ_{hv} and LDR would *not* deviate measurably in rain, even for large drops at X band. At S band, the same is true for δ, ρ_{hv}, and LDR. Therefore, the identification of large drop cores at S band is complicated compared to C and X bands. We suggest using the propagation-affected Z_{dr} and Z_h for identifying large drop cores at S band. Because the overall propagation effects are less at S band in comparison with lower wavelengths, we believe that most large drop cores should still be identifiable from the uncorrected Z_h and Z_{dr} at S band.

Acknowledgments. We wish to thank Mr. Ken Glasson of the Bureau of Meteorology Research Centre for his superlative engineering work in developing and deploying the C-pol radar for the Maritime Continent Thunderstorm Experiment. We also thank Mr. John Lutz and Dr. Jeffrey Keeler of the National Center for Atmospheric Research for their efforts in improving the performance of the C-pol radar. We acknowledge Dr. Tsutomu Takahashi for providing the analyzed videosonde data. The support of the Tiwi Land Council in undertaking MCTEX is acknowledged. We would like to recognize helpful discussions regarding propagation effects in polarimetric radar data with Drs. Peter May, Dusan Zrnić, V. N. Bringi, and Anthony Illingworth. This research was supported by NASA TRMM Grants NAG 5-2692 and NAG5-4754 and NSF Grant ATM-9726464.

APPENDIX A

Polarimetric Radar Data Processing

Before analyzing any C-pol radar observations, all data were carefully edited using the Research Data Support System (RDSS) software developed at the National Center for Atmospheric Research (NCAR) (Oye and Carbone 1981). First, all polarimetric radar data (Z_h, Z_{dr}, Ψ_{dp}, and ρ_{hv}) at range gates characterized by $\rho_{hv} < 0.7$ were removed. This ρ_{hv} thresholding technique removes range gates in which the returned power is dominated by unacceptably low signal-to-noise ratios or by ground clutter (Ryzhkov and Zrnić 1998b). Any remaining ground clutter was manually removed since it has a deleterious effect on the quality of polarimetric radar measurements at low elevation angles. Spurious values of horizontal reflectivity and differential reflectivity caused by three-body scattering effects (Zrnić 1987; Hubbert and Bringi 1997) were removed manually. In regions of large reflectivity gradients, antenna pattern–induced errors can bias the estimates of Z_{dr}, ρ_{hv}, and to a lesser extent Ψ_{dp} (Pointin et al. 1988). In order to remove spurious data, we manually examined all regions of large ∇Z_h (>20 dBZ km^{-1}) in azimuth and elevation and deleted the data if it appeared suspect. During MCTEX, the C-pol differential phase data were recorded between -32° and $+32^\circ$ with folding occurring for values outside of these bounds (Keenan et al. 1998). A dealiasing algorithm in the RDSS software package was used to unfold the Ψ_{dp} data. Next, the horizontal reflectivity data at low elevation angles ($<4^\circ$) were corrected for partial beam blocking according to the procedure described in May et al. (1999). We then

removed the bias in Z_{dr} of +0.1 dB as determined from a vertically pointing scan in stratiform precipitation on 29 November 95 (Keenan et al. 1998).

Because the differential phase at C band is a combination of both the backscatter differential phase, which can be significant at C band (e.g., Bringi et al. 1990, 1991; Aydin and Giridhar 1992), and the (forward) propagation differential phase, it was necessary to apply an iterative filtering technique (Hubbert and Bringi 1995) to the differential phase data. We utilized a 13-point (over 3.9 km) running mean filter. The iterative application of this filter was designed to remove gate-to-gate fluctuations caused by significant δ or system phase noise while preserving the physically meaningful trends caused by ϕ_{dp}. The specific differential phase was then calculated from the filtered differential phase using a finite differencing approximation according to (4). The accuracy or standard deviation of K_{dp} can be estimated from the expression given by Balakrishnan and Zrnić (1990)

$$\sigma_{K_{dp}} = \frac{\sqrt{3}\sigma_{dp}}{N^{3/2}\Delta_r}, \tag{A1}$$

where σ_{dp} is the standard deviation of the differential phase, N is the number of range gates in the filter, and Δ_r is the range gate spacing. Given a standard deviation of the differential phase of about 3°–4° (Keenan et al. 1998), 13 points in the filter, and a range gate spacing of 0.3 km, the accuracy of K_{dp} is estimated as 0.4–0.5° km^{-1}. For the dwell times used in this study (128 samples and azimuthal rotation rates from 6° to 8° s^{-1}), typical standard errors of measurement for the other variables are: 1 dBZ for Z_h, 0.25 dB for Z_{dr}, and 0.01 for ρ_{hv} (Keenan et al. 1998).

Some analysis applications in this study required gridded Cartesian radar data. Therefore, we interpolated all polarimetric radar variables to a Cartesian grid using the NCAR REORDER software package (Mohr 1986). The grid was centered on the Tiwi Islands with a horizontal and vertical spacing of 1.0 and 0.5 km, respectively. Variable radii of influence consistent with the scanning strategies during MCTEX (Keenan et al. 1994) were utilized in order to maximize the resolution of the data in range from the radar. The radius of influence in the azimuthal (elevational) direction was 1.2° (2°). In range, the radius of influence was equal to the product of the range and the azimuthal radius of influence in radians.

APPENDIX B

Scattering Simulations of C-Band Polarimetric Radar Parameters in Rain

During MCTEX, a Joss and Waldvogel (1967) disdrometer collected raindrop size distribution information as described in Keenan et al. (1999). The disdrometer data were fit to gamma drop size distributions according to Ulbrich (1983). As discussed in KCZM, empirical linear relationships between the gamma DSD parameters were determined. The empirical relations were then used to obtain physically realistic domains for the fitted gamma DSD parameters that were used as input to the T-matrix (Barber and Yeh 1975) scattering simulations of rainfall at C band (5.33 cm).

In the T-matrix scattering simulations, raindrops were modeled as oblate spheroids with a shape versus size relationship defined by Green (1975). The dielectric of water was obtained from Ray (1972) using a temperature of 20°C, consistent with typical wet-bulb temperatures near the surface over the Tiwi Islands as analyzed from sounding data during MCTEX. Based on in situ and radar observations of large drops during MCTEX and prior evidence for the presence of large drops in tropical convection (reference summary in appendix C), the maximum drop diameter D_{max} was set at 8 mm and the median volume diameter D_0 was allowed to vary from 0.8 to 5 mm. As discussed above, the other DSD parameters (N_0, μ) of a gamma distribution were varied according to empirical relationships determined by KCZM.

Using the resulting T matrices as input to a Muellermatrix scattering model (e.g., Vivekanandan et al. 1991), C-band backscatter and propagation characteristics as described by various polarimetric radar parameters (Z_h, Z_{dr}, K_{dp}, δ, ρ_{hv}, A_h, and A_{hv}) were simulated. Following Vivekanandan et al. (1991), hydrometeor canting angle and radar elevation angle effects were considered. Rainfall orientation distributions were modeled by a quasi-Gaussian distribution (e.g., Vivekanandan et al. 1991) with a mean of zero and a standard deviation of 5°. For the results in this study, the simulated radar elevation angle was held fixed in a plane 0.5° above the local surface.

APPENDIX C

In situ and Radar Evidence of Large Drops during MCTEX

Before offering observational evidence supporting the presence of large (i.e., $D > 3$ mm) drops in the tropical island convection observed during MCTEX, it is important to review some potential hypotheses for their production. In tropical maritime air masses, the presence of exceptionally large aerosol particles acting as nuclei for drops near cloud base may allow drops to reach giant size (5–8 mm) as they accrete smaller drops (e.g., Johnson 1982; Rauber et al. 1991; Szumowski et al. 1999). Alternatively in the Tropics, an active coalescence process in a cloud environment nearly devoid of smaller raindrops, hence limiting collisional breakup, but rich in cloud liquid water can result in large drop production (e.g., Rauber et al. 1991; Szumowski et al. 1998). Although it is beyond the scope of this study to investigate these hypotheses further, it is possible that

one or both of these mechanisms were operative over the Tiwi Islands during MCTEX.

Both in situ and polarimetric radar data collected during MCTEX suggest the presence of large raindrops. A videosonde system described by Takahashi (1990) collected in situ microphysical data during MCTEX. During six in-cloud ascents in various microphysical conditions, the videosonde observations confirmed the presence of large raindrops in tropical convection. Despite the small sample size of the instrument and a limited number of cloud ascents in microphysical regions typically associated with large drops (T. Takahashi 1997, personal communication), a significant number of large raindrops were observed. A total of 21 (5) drops possessing diameters in excess of 3 mm (5 mm) and 1 drop with a diameter of 8 mm were observed with the videosonde system. In addition, a Joss and Waldvogel (1967) disdrometer collected raindrop information at the surface during MCTEX. Despite a small sample volume, the disdrometer observed 12 drops with diameters in excess of 5 mm (KCZM). Disdrometer data collected during 1998 over Darwin, Australia, and during the South China Sea Mesoscale Experiment provide further evidence of large drops in tropical convection. Similarly, preliminary analyses of disdrometer observations from Brazil during the Tropical Rainfall Measuring Mission Large Biosphere–Atmosphere experiment (January–February 1999) support the existence of large drops ($D > 5$ mm) in the Tropics (J. Hubbert 1999, personal communication). These data are consistent with in situ aircraft observations of large drops (i.e., 4–8 mm in diameter) coincident with high reflectivity cores in rainbands over Hawaii (Beard et al. 1986; Szumowski et al. 1998).

During MCTEX, the C-pol radar observed maximum values of Z_{dr} in excess of 5 dB, suggesting the presence of raindrops possessing $D_0 > 4$ mm and $D_{max} \geq 6$ mm. At 0416 UTC, there were more than 12 distinct precipitation cores with $Z_{dr} \geq 3$ dB at 2 km AGL (Fig. 7b). Rain cores characterized by $Z_{dr} \geq 3$ dB (and hence $D_0 > 2.5$ mm) were observed *routinely* by the C-pol radar during the developing to mature phase of the 28 November 1995 tropical convective system. From 0216 to 0626 UTC, these large drop precipitation cores covered from 12 to 74 km^2 of surface area, representing 1 to 6% of the convective ($Z_h > 25$ dBZ) precipitation echo at 0.5 km AGL. Illingworth et al. (1987) found similar polarimetric radar evidence of large raindrops ($D > 4$ mm) in developing cumulonimbus clouds.

To demonstrate that large drops were also a significant component of the propagation medium, we partitioned the storm integrated K_{dp} by Z_{dr} for the developing to mature phase (0216–0626 UTC) of the convection below 3 km (Fig. C1). Because Z_{dr} is a measure of the reflectivity-weighted drop shape (Jameson 1983) and hence size (e.g., Pruppacher and Beard 1970), and K_{dp} is proportional to the specific horizontal and differential attenuation (Bringi et al. 1990), the results in Fig. C1

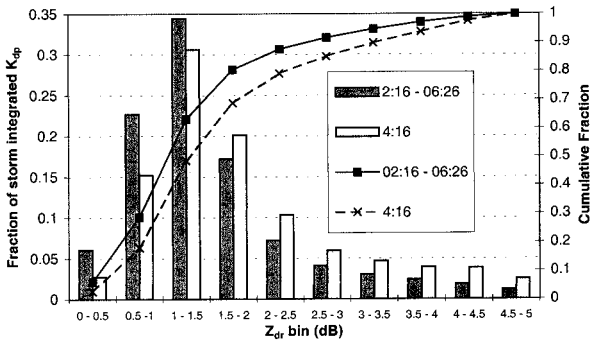

FIG. C1. Histogram of the storm integrated specific differential phase (K_{dp}) vs the median differential reflectivity (Z_{dr}, dB) of each Z_{dr} bin for 0416 UTC and the mean conditions from 0216 to 0626 UTC on 28 Nov 1995 below 3 km. The storm-integrated K_{dp} fraction for each 0.5 dB Z_{dr} bin was calculated by adding K_{dp} at each range gate below 3 km to the appropriate bin sum and then dividing the bin sum by the storm total K_{dp} sum below 3 km.

provide a rough estimate of the role large drops played in propagation effects. As expected, a large majority (74%) of the storm-integrated K_{dp} from 0216 to 0626 UTC was caused by drops with small to moderate Z_{dr} ($0.5 < Z_{dr} < 2.0$ dB). However, over 20% of the storm-integrated K_{dp} was caused by rainfall characterized by large $Z_{dr} > 2$ dB. During the most intense period of the mature phase (e.g., 0416 UTC as shown in Figs. 6 and 7a,b), 31% of the storm-integrated K_{dp} was caused by large drops ($Z_{dr} > 2$ dB). Of course, the juxtaposition of these large drop cores between the radar and the rest of the precipitation echo will also determine how important they are in causing propagation effects. On 28 November 1995, much of the intense convection developed close to the radar with significant echo downrange from large drop cores (cf. Figs. 7a,b). Therefore, large drops did play an important role in the propagation medium over the Tiwi Islands.

REFERENCES

Atlas, D., and H. C. Banks, 1951: The interpretation of microwave reflections from rainfall. *J. Meteor.,* **8,** 271–282.

Aydin, K., and V. Giridhar, 1992: C-band dual-polarization radar observables in rain. *J. Atmos. Oceanic Technol.,* **9,** 383–390.

——, Y. Zhao, and T. A. Seliga, 1989: Rain-induced attenuation effects on C-band dual-polarization meteorological radars. *IEEE Trans. Geosci. Remote Sens.,* **27,** 57–66.

Balakrishnan, N., and D. S. Zrnić, 1989: Correction of propagation effects at attenuating wavelengths in polarimetric radars. Preprints, *24th Conf. on Radar Meteorology,* Tallahassee, FL, Amer. Meteor. Soc., 287–291.

——, and ——, 1990: Estimation of rain and hail rates in mixed-phase precipitation. *J. Atmos. Sci.,* **47,** 565–583.

Barber, P., and C. Yeh, 1975: Scattering of electromagnetic waves by arbitrarily shaped dielectric bodies. *Appl. Opt.,* **14,** 2864–2872.

Beard, K. V., D. B. Johnson, and D. Baumgardner, 1986: Aircraft observations of large raindrops in warm, shallow, convective clouds. *Geophys. Res. Lett.,* **13,** 991–994.

Bolen, S., V. N. Bringi, and V. Chandrasekar, 1998: An optimal area approach to intercomparing polarimetric radar rain-rate algo-

rithms with gauge data. *J. Atmos. Oceanic Technol.,* **15,** 605–623.

Bringi, V. N., and A. Hendry, 1990: Technology of polarization diversity radars for meteorology. *Radar in Meteorology: Battan Memorial and 40th Anniversary Radar Meteorology Conference,* D. Atlas, Ed., Amer. Meteor. Soc., 153–190.

——, V. Chandrasekar, N. Balakrishnan, and D. S. Zrnić, 1990: An examination of propagation effects in rainfall on radar measurements at microwave frequencies. *J. Atmos. Oceanic Technol.,* **7,** 829–840.

——, ——, P. Meischner, J. Hubbert, and Y. Golestani, 1991: Polarimetric radar signatures of precipitation at S- and C-bands. *IEE Proc. F,* **138,** 109–119.

Carey, L. D., 1999: On the relationship between precipitation and lightning as revealed by multiparameter radar observations. Ph.D. dissertation, Colorado State University, 238 pp.

——, and S. A. Rutledge, 2000: The relationship between precipitation and lightning in tropical island convection: A C-band polarimetric radar study. *Mon. Wea. Rev.,* **128,** 2687–2710.

Gorgucci, E., G. Scarchilli, and V. Chandrasekar, 1996: Error structure of radar rainfall measurement at C-band frequencies with dual polarization algorithm for attenuation correction. *J. Geophys. Res.,* **101,** 26 461–26 472.

——, ——, ——, P. F. Meischner, and M. Hagen, 1998: Intercomparison of techniques to correct for attenuation of C-band weather radar signals. *J. Appl. Meteor.,* **37,** 845–853.

Green, A. W., 1975: An approximation for the shape of large raindrops. *J. Appl. Meteor.,* **14,** 1578–1583.

Gunn, K. L. S., and T. W. R. East, 1954: The microwave properties of precipitation particles. *Quart. J. Roy. Meteor. Soc.,* **80,** 522–545.

Hildebrand, P. H., 1978: Iterative correction for attenuation of 5 cm radar in rain. *J. Appl. Meteor.,* **17,** 508–514.

Hitschfeld, W., and J. Bordan, 1954: Errors inherent in the radar measurement of rainfall at attenuating wavelengths. *J. Meteor.,* **11,** 58–67.

Holt, A. R., 1988: Extraction of differential propagation phase from data from S-band circularly polarized radars. *Electron. Lett.,* **24,** 1241–1242.

Hubbert, J., and V. N. Bringi, 1995: An iterative filtering technique for the analysis of copolar differential phase and dual-frequency radar measurements. *J. Atmos. Oceanic Technol.,* **12,** 643–648.

——, and ——, 1997: The effects of 3-body scattering on differential reflectivity. Preprints, *28th Conf. on Radar Meteorology,* Austin, TX, Amer. Meteor. Soc., 11–12.

——, V. Chandrasekar, V. N. Bringi, P. Meischner, 1993: Processing and interpretation of coherent dual-polarized radar measurements. *J. Atmos. Oceanic Technol.,* **10,** 155–164.

Illingworth, A. J., J. W. Goddard, and S. M. Cherry, 1987: Polarization radar studies of precipitation development in convective storms. *Quart. J. Roy. Meteor. Soc.,* **113,** 469–489.

Jameson, A. R., 1991a: Polarization radar measurements in rain at 5 and 9 GHz. *J. Appl. Meteor.,* **30,** 1500–1513.

——, 1991b: A comparison of microwave techniques for measuring rainfall. *J. Appl. Meteor.,* **30,** 32–54.

——, 1992: The effect of temperature on attenuation-correction schemes in rain using polarization propagation differential phase shift. *J. Appl. Meteor.,* **31,** 1106–1118.

——, and E. A. Mueller, 1985: Estimation of differential phase shift from sequential orthogonal linear polarization radar measurements. *J. Atmos. Oceanic Technol.,* **2,** 133–137.

Johnson, B. C., and E. A. Brandes, 1987: Attenuation of a 5-cm wavelength radar signal in the Lahoma–Orienta storms. *J. Atmos. Oceanic Technol.,* **4,** 512–517.

Johnson, D. B., 1982: The role of giant and ultragiant aerosol particles in warm rain initiation. *J. Atmos. Sci.,* **39,** 448–460.

Joss, V. J., and A. Waldvogel, 1967: Ein spectograph fur Niederschlagstropher mit automatischer auswertung. *Pure Appl. Geophys.,* **68,** 240–246.

Keenan, T. D., and Coauthors, 1994: Science Plan—Maritime Continent Thunderstorm Experiment. BMRC Research Rep. 44, 61 pp. [Available from Bureau of Meteorology Research Centre, P.O. Box 1289K, Melbourne, Victoria 3001, Australia.]

——, R. Carbone, S. Rutledge, J. Wilson, G. Holland, and P. May, 1996: The Maritime Continent Thunderstorm Experiment (MCTEX): Overview and initial results. Preprints, *Seventh Conf. on Mesoscale Processes,* Reading, United Kingdom, Amer. Meteor. Soc., 326–328.

——, K. Glasson, F. Cummings, T. S. Bird, J. Keeler, and J. Lutz, 1998: The BMRC/NCAR C-band polarimetric (C-POL) radar system. *J. Atmos. Oceanic Technol.,* **15,** 871–886.

——, L. D. Carey, D. S. Zrnić, and P. T. May, 2000: Sensitivity of 5-cm wavelength polarimetric radar variables to raindrop axial ratio and drop size distribution. *J. Appl. Meteor.,* in press.

May, P. T., T. D. Keenan, D. S. Zrnić, L. D. Carey, and S. A. Rutledge, 1999: Polarimetric radar measurements of tropical rain at a 5-cm wavelength. *J. Appl. Meteor.,* **38,** 750–765.

Mohr, C. G., 1986: Merger of mesoscale data sets into a common Cartesian format for efficient and systematic analyses. *J. Atmos. Oceanic. Technol.,* **3,** 143–161.

Oguchi, T., 1983: Electromagnetic wave propagation and scattering in rain and other hydrometeors. *IEEE Proc.,* **71,** 1029–1078.

Oye, R., and R. E. Carbone, 1981: Interactive Doppler editing software. *Proc. 20th Conf. on Radar Meteorology,* Boston, MA, Amer. Meteor. Soc., 683–689.

Pointin, Y. C., C. Ramond, and J. Fournet-Fayard, 1988: Radar differential reflectivity Z_{dr}: A real case evaluation of errors induced by antenna characteristic. *J. Atmos. Oceanic Technol.,* **5,** 416–423.

Pruppacher, H. R., and K. V. Beard, 1970: A wind tunnel investigation of the internal circulation and shape of water drops falling at terminal velocity in air. *Quart. J. Roy. Meteor. Soc.,* **96,** 247–256.

Rauber, R. M., K. V. Beard, and B. M. Andrews, 1991: A mechanism for giant raindrop formation in warm, shallow, convective clouds. *J. Atmos. Sci.,* **48,** 1791–1797.

Ray, P. S., 1972: Broad-band complex refractive indices of ice and water. *Appl. Opt.,* **11,** 1836–1844.

Ryde, J. W., 1946: The attenuation and radar echoes produced at centimetre wavelengths by various meteorological phenomena. *Meteorological Factors in Radio Wave Propagation,* Physical Society, 169–189.

Ryzhkov, A. V., and D. S. Zrnić, 1994: Precipitation observed in Oklahoma mesoscale convective systems with a polarimetric radar. *J. Appl. Meteor.,* **33,** 455–464.

——, and ——, 1995a: Precipitation and attenuation measurements at a 10-cm wavelength. *J. Appl. Meteor.,* **34,** 2121–2134.

——, and ——, 1995b: Comparison of dual-polarization radar estimators of rain. *J. Atmos. Oceanic Technol.,* **12,** 249–256.

——, and ——, 1996a: Rain in shallow and deep convection measured with a polarimetric radar. *J. Atmos. Sci.,* **53,** 2989–2995.

——, and ——, 1996b: Assessment of rainfall measurement that uses specific differential phase. *J. Appl. Meteor.,* **35,** 2080–2090.

——, and ——, 1998a: Beamwidth effects on the differential phase measurements of rain. *J. Atmos. Oceanic Technol.,* **15,** 624–634.

——, and ——, 1998b: Polarimetric rainfall estimation in the presence of anomalous propagation. *J. Atmos. Oceanic Technol.,* **15,** 1320–1330.

——, ——, and D. Atlas, 1997: Polarimetrically tuned $R(Z)$ relations and comparisons of radar rainfall methods. *J. Appl. Meteor.,* **36,** 340–349.

Scarchilli, G., E. Gorgucci, V. Chandrasekar, and T. A. Seliga, 1993: Rainfall estimation using polarimetric techniques at C-band frequencies. *J. Appl. Meteor.,* **32,** 1150–1160.

Shepherd, G. W., J. Searson, A. Pallot, and C. G. Collier, 1995: The performance of a C-band weather radar during a line convection event. *Meteor. Appl.,* **2,** 65–69.

Smyth, T. J., and A. J. Illingworth, 1998: Correction for attenuation of radar reflectivity using polarisation data. *Quart. J. Roy. Meteor. Soc.,* **124,** 2393–2415.

Szumowski, M. J., R. M. Rauber, H. T. Ochs III, and K. V. Beard, 1998: The microphysical structure and evolution of Hawaiian rainband clouds. Part II: Aircraft measurements within rainbands containing high reflectivity cores. *J. Atmos. Sci.,* **55,** 208–226.

——, ——, and ——, 1999: The microphysical structure and evolution of Hawaiian rainband clouds. Part III: A test of the ultragiant nuclei hypothesis. *J. Atmos. Sci.,* **56,** 1980–2003.

Takahashi, T., 1990: Near absence of lightning in torrential rainfall producing Micronesian thunderstorms. *Geophys. Res. Lett.,* **17,** 2381–2384.

Tan, J., J. W. F. Goddard, and M. Thurai, 1995: Applications of differential propagation phase in polarisation-diversity radars at S-band and C-band. *Proc. Ninth Int. Conf. on Antenna and Propagation,* Eindhoven, Netherlands, IEE, IEE Conference Publication 407, 336–341.

Ulbrich, C. W., 1983: Natural variations in the analytical form of the raindrop size distribution. *J. Climate Appl. Meteor.,* **22,** 1764–1775.

Vivekanandan, J., W. M. Adams, and V. N. Bringi, 1991: Rigorous approach to polarimetric radar modeling of hydrometeor orientation distributions. *J. Appl. Meteor.,* **30,** 1053–1063.

Yuter, S. E., and R. A. Houze Jr., 1995: Three-dimensional kinematic and microphysical evolution of Florida cumulonimbus. Part II: Frequency distributions of vertical velocity, reflectivity, and differential reflectivity. *Mon. Wea. Rev.,* **123,** 1941–1963.

Zawadzki, I., 1975: On radar–raingage comparison. *J. Appl. Meteor.,* **14,** 1430–1436.

——, 1984: Factors affecting the precision of radar measurements of rain. Preprints, *22d Conf. on Radar Meteorology,* Zurich, Switzerland, Amer. Meteor. Soc., 251–256.

Zrnić, D. S., 1987: Three-body scattering produces precipitation signature of special diagnostic value. *Radio Sci.,* **22,** 76–86.

——, and A. V. Ryzhkov, 1996: Advantages of rain measurements using specific differential phase. *J. Atmos. Oceanic Technol.,* **13,** 465–476.

——, and ——, 1997: Polarimetric measurements of rain. *Weather Radar Technology for Water Resources Management,* B. Braga and O. Massambani, Eds., UNESCO Press, 77–86.

——, T. D. Keenan, L. D. Carey, and P. T. May, 2000: Sensitivity analysis of polarimetric variables at a 5-cm wavelength in rain. *J. Appl. Meteor.,* **39,** 1514–1526.